membranes. Membranes were then hybridized with ^{32}P-labeled probe, washed and autoradiographed.

Northern blot hybridization
RNA isolated using an SV total RNA isolation kit (Promega, Madison, WI, USA) was subjected to formaldehyde-1.2% agarose gel electrophoresis, blotted onto nylon membranes, hybridized with ^{32}P-labeled probe, washed and autoradiographed.

Construction of retrovirus vector and virus production
pCX4bsr, a Moloney murine leukemia virus-based retrovirus vector containing the blasticidin S resistance gene (*bsr*) as a selectable marker, was constructed by Akagi *et al.* (2000). pCX4-CapG was constructed by inserting full-length human CapG cDNA into the multi-cloning site of the pCX4bsr vector.

Phoenix-A cells were transfected with pCX4bsr or pCX4-CapG constructs using FuGene 6 (Roche Diagnostics, Mannheim, Germany) according to the manufacturer's protocols. Two days after transfection, the culture supernatants were collected and stored at −70°C until use.

Tumorigenicity in nude mice
Female 4-week-old BALB/cJ (nu/nu) mice were injected subcutaneously in the back with CapG- or empty virus-infected cells in 0.2 ml of DMEM (without serum). After 7 weeks, tumor size was measured in two dimensions using hand calipers, and tumor volume calculated by the formula $0.5 \times L \times W^2$, where L and W are the length and width of a tumor, respectively (Sagawa *et al*, 2003).

Anchorage-independent growth assay
Anchorage-independent growth was assessed by colony-forming ability in soft agar. Ten thousand cells were inoculated into 0.35% agarose in DMEM supplemented with 10% FBS per 60 mm dish. After 2 weeks' incubation, the number of colonies (> 0.125 mm in diameter) was scored.

Cell migration assay
Cells (4×10^4) were suspended in 200 μl of serum-free DMEM containing 0.1% bovine serum albumin, and plated in upper chamber of Chemotaxicell (Kurabo, Osaka, Japan). The lower chamber contained 600 μl of phosphate-buffered saline supplemented with 6 μg/ml fibronectin. After incubation for 6 h at 37°C, cells were fixed with 80% methanol, and stained with hematoxylin. The number of cells migrated through membrane was counted under microscope.

Acknowledgements

We thank Dr Akagi for providing the pCX4 retrovirus vector. SH is a recipient of a grant from the Charitable Trust Osaka Cancer Researcher-Fund.

References

Akagi T, Shishido T, Murata K, Hanafusa H. (2000). *Proc Natl Acad Sci USA* **97**: 7290–7295.
Dabiri GA, Young CL, Rosenbloom J, Southwick FS. (1992). *J Biol Chem* **267**: 16545–16552.
Davies H, Bignell GR, Cox C, Stephens P, Edkins S, Clegg S *et al* (2002). *Nature* **417**: 949–954.
De Corte V, Van Impe K, Bruyneel E, Boucherie C, Mareel M, Vandekerckhove J *et al.* (2004). *J Cell Sci* **117**: 5283–5292.
Hahn WC, Weinberg RA. (2002). *Nat Rev Cancer* **2**: 331–341.
Lal A, Lash AE, Altschul SF, Velculescu V, Zhang L, McLendon RE *et al.* (1999). *Cancer Res* **59**: 5403–5407.
Oka K, Tomonaga Y, Nakazawa T, Ge H-Y, Bengtsson U, Stanbridge EJ *et al.* (1999). *Genes, Chromosome Cancer* **26**: 47–53.
Pellieux C, Desgeorges A, Pigeon CH, Chambaz C, Yin H, Hayoz D *et al.* (2003). *J Biol Chem* **278**: 29136–29144.
Prendergast GC, Ziff EB. (1991). *EMBO J* **10**: 757–766.
Rajagopalan H, Bardelli A, Lengauer C, Kinzler KW, Vogelstein B, Velculescu VE. (2002). *Nature* **418**: 934.
Rajogopalan H, Nowak MA, Vogelstein B, Lengauer C. (2003). *Nat Rev Cancer* **3**: 695–701.
Sagawa N, Fujita H, Banno Y, Nozawa Y, Katoh H, Kuzumaki N. (2003). *Br J Cancer* **88**: 606–612.
Silacci P, Mazzolai L, Gauci C, Stergiopulos N, Yin HL, Hayoz D. (2004). *Cell Mol Life Sci* **61**: 2614–2623.
Tanaka M, Mullauer L, Ogiso Y, Fujita H, Moriya S, Furuuchi K *et al.* (1995). *Cancer Res* **55**: 3228–3232.
Van Ginkel PR, Gee RL, Walker TM, Hu D-N, Heizmann CW, Polans AS. (1998). *Biochim Biophys Acta* **1448**: 290–297.
Yu F-X, Johnston PA, Sudhof TC, Yin HL. (1990). *Science* **250**: 1413–1415.

Supplementary Information accompanies the paper on the Oncogene website (http://www.nature.com/onc).

RAPID COMMUNICATIONS IN MASS SPECTROMETRY
Rapid Commun. Mass Spectrom. 2006; **20**: 2589–2595
Published online in Wiley InterScience (www.interscience.wiley.com). DOI: 10.1002/rcm.2595

RCM

'Information-Based-Acquisition' (IBA) technique with an ion-trap/time-of-flight mass spectrometer for high-throughput and reliable protein profiling

Toshiyuki Yokosuka[1]*, Kiyomi Yoshinari[1], Kinya Kobayashi[1], Atsushi Ohtake[1], Atsumu Hirabayashi[2], Yuichiro Hashimoto[2], Izumi Waki[2] and Toshifumi Takao[3]

[1]Hitachi Research Laboratory, Hitachi, Ltd., Omika 7-1-1, Hitachi, Ibaraki 319-1292, Japan
[2]Central Research Laboratory, Hitachi, Ltd., Higashi-Koigakubo 1-280, Kokubunji, Tokyo 185-8601, Japan
[3]Institute for Protein Research, Osaka University, Yamadaoka 3-2, Suita, Osaka 565-0871, Japan

Received 26 December 2005; Revised 1 June 2006; Accepted 2 June 2006

Highly complex protein mixtures can be analyzed after proteolysis using liquid chromatography/mass spectrometry (LC/MS). In an LC/MS run, intense peptide ions originating from high-abundance proteins are preferentially analyzed using tandem mass spectrometry (MS^2), so obtaining the MS^2 spectra of peptide ions from low-abundance proteins is difficult even if such ions are detected. Furthermore, the MS^2 spectra may produce insufficient information to identify the peptides or proteins. To solve these problems, we have developed a real-time optimization technique for MS^2, called the Information-Based-Acquisition (IBA) system. In a preliminary LC/MS run, a few of the most intense ions detected in every MS spectrum are selected as precursors for MS^2 and their masses, charge states and retention times are automatically registered in an internal database. In the next run, a sample similar to that used in the first run is analyzed using database searching. Then, the ions registered in the database are excluded from the precursor ion selection to avoid duplicate MS^2 analyses. Furthermore, real-time *de novo* sequencing is performed just after obtaining the MS^2 spectrum, and an MS^3 spectrum is obtained for accurate peptide identification when the number of interpreted amino acids in the MS^2 spectrum is less than five. We applied the IBA system to a yeast cell lysate which is a typical crude sample, using a nanoLC/ion-trap time-of flight (IT/TOF) mass spectrometer, repeating the same LC/MS run five times. The obtained MS^2 and MS^3 spectra were analyzed by applying the Mascot® (Matrix Science, Boston, MA, USA) search engine to identify proteins from the sequence database. The total number of identified proteins in five LC/MS runs was three times higher than that in the first run and the ion scores for peptide identification also significantly increased, by about 70%, when the MS^3 spectra were used, combined with the MS^2 spectra, before being subjected to Mascot® analysis. Copyright © 2006 John Wiley & Sons, Ltd.

Highly complex protein mixtures can be analyzed after proteolysis using liquid chromatography/mass spectrometry (LC/MS). Recently, special attention has been paid to the analysis of the low-abundance proteins that are thought to relate to diseases. However, in an LC/MS run, the peptide ions originating from high-abundance proteins are preferentially analyzed by tandem mass spectrometry (MS^2). It is difficult to obtain MS^2 spectra of peptide ions from low-abundant proteins even if the ions are detected. This is because only a limited number of ions are selected as precursors of the MS^2 analyses. In general, it is necessary to separate the crude sample to reduce the influence of the high-abundance proteins using gel electrophoresis or multi-dimensional LC/MS thus spending a good deal of time in complex preprocessing. Furthermore, there is the problem that the analysis of the further low-abundance proteins will become difficult using the current method when the sensitivity of mass spectrometer improves. Therefore, in order to increase the throughput of the analysis of low-abundance proteins, it is necessary to reduce the number of LC/MS runs, and ions detected in MS, which were previously selected as MS^2 precursor ions, should be excluded from subsequent MS^2 precursor ion candidates.

So far, a number of different approaches have been employed to identify proteins from the MS^2 spectra. The most common approaches rely on available databases to match the experimental MS^2 spectra.[1,2] However, some MS^2 spectra may have insufficient information to identify the peptides or proteins, as in the reported cases of neutral loss or non-mobile protons.[3–9] MS^2 data do not always provide

*Correspondence to: T. Yokosuka, Hitachi Research Laboratory, Hitachi, Ltd., Omika 7-1-1, Hitachi, Ibaraki 319-1292, Japan.
E-mail: toshiyuki.yokosuka.gc@hitachi.com
Contract/grant sponsors: Hitachi High Technologies, Ltd; New Energy and Industrial Technology Development Organization (NEDO).

sufficient fragment ion peaks for identifying peptides with a high accuracy. In such cases, MS^3 analysis, which is a technique that could obtain more information about fragment species of a precursor ion, will be efficient for identifying as many peptides in a mixture as possible. However, MS^3 analysis usually requires more time than MS^2 analysis. Therefore, unnecessary MS^3 analysis reduces the total throughput of the MS analysis. So, it is necessary to judge whether the MS^2 spectrum have sufficient information to identify the peptides during the measurement, and MS^3 analysis should be performed only when it is needed.

In this paper we describe a new approach using software, called Information-Based-Acquisition (IBA), in which the sequence of tandem mass spectrometry is automatically optimized, so that precursor ions should be selected to increase identified proteins with high accuracy.

INFORMATION-BASED ACQUISITION (IBA)

Figure 1 shows the workflow for protein profiling with an ion trap time-of-flight (IT/TOF) mass spectrometer controlled by the IBA system. The IBA, which is a real time-optimization technique for tandem mass spectrometry (MS^2), consists of the following two main functions: (1) precursor ion selection with an internal database for MS data, and (2) automated MS^3 analysis with real-time *de novo* sequencing[10–13] for MS^2 spectra. To perform real-time optimization, it is preferable that the processing time for optimization is within 10 ms which is negligible enough for actual MS measurement. The features of each function are as follows.

Precursor ion selection with an internal database (IBA (I))

IBA (I) judges whether an ion species has already been analyzed in order to avoid duplicate analysis. Figure 2 shows the processing flow of IBA (I). The approach taken in IBA (I) can be summarized into three steps: (i) preprocessing, (ii) database searching, and (iii) scoring and selecting precursor ions.

(i) The first step consists of preprocessing of the raw MS data. This involves a new method for noise filtering (1-1), peak centering, as well as deconvolution of the multiply charged species to a neutral mass value (1-2). This step is very important for the judgment of the information on the ions. Therefore, optimal preprocessing of the data is the most important step for precursor ion selection with internal database searching. To verify the judgment accuracy of preprocessing, we applied our algorithm to 278 peaks included in the same spectra extracted at random from the LC/MS data of bovine serum albumin (BSA) digested by trypsin and checked them by the visual evaluation. The judgment accuracy of ion information using IBA, such as monoisotopic mass value and charge state, is more than 90%.

(ii) The second step is database searching (1-3). IBA gives a score to an ion only when the data set (mass value (m), retention time (RT) and charge state (z)) of the ion does not agree with the data set of the internal database, or a fixed time after the ion begins to be detected, or until the integrated value of the analyzed ion intensity becomes a definite value. The data set of the MS^2 precursor ions is automatically stored in the internal database (DB) which can currently store 40 000 data points for MS^2 precursor ions. The storage capacity of the system can be increased if necessary. In particular, judgment of the integrated value of the analyzed ion's intensity is effective for the analysis of low-abundance species. Because the signal-to-noise (S/N) ratio of the MS^2 spectra of low-abundance species is very poor, it is preferable to measure over a long time period in order to improve the S/N ratio by summing of spectra.

(iii) The third step is scoring and selection of the next MS^2 precursor ion. The intensity of the ion is scored (1-4). If the

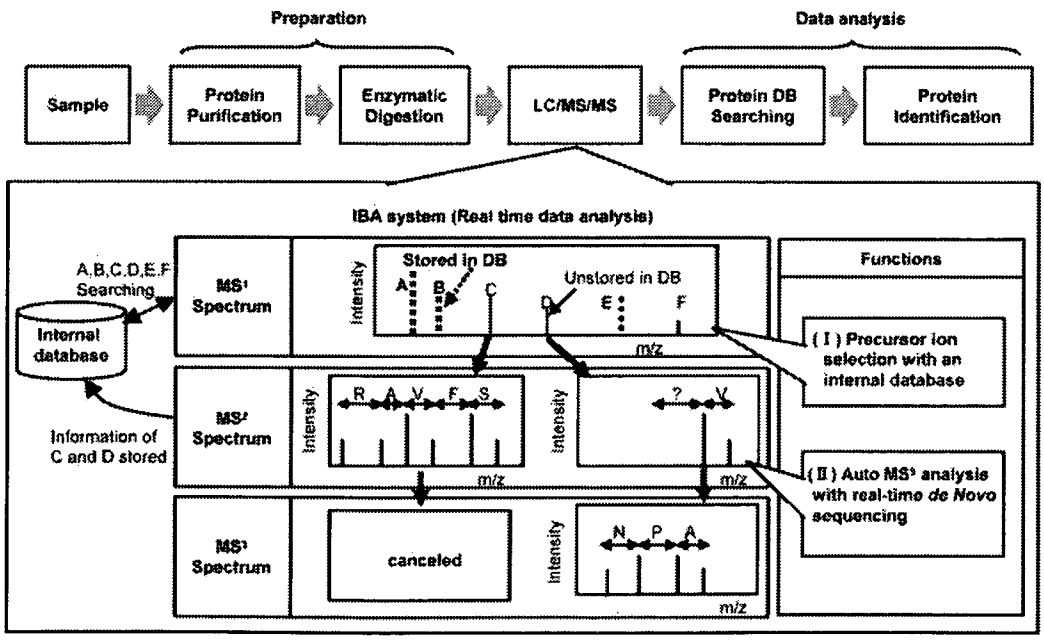

Figure 1. The workflow for protein profiling with an IT-TOF mass spectrometer controlled by an Information-Based-Acquisition (IBA) system.

DOI: 10.1002/rcm

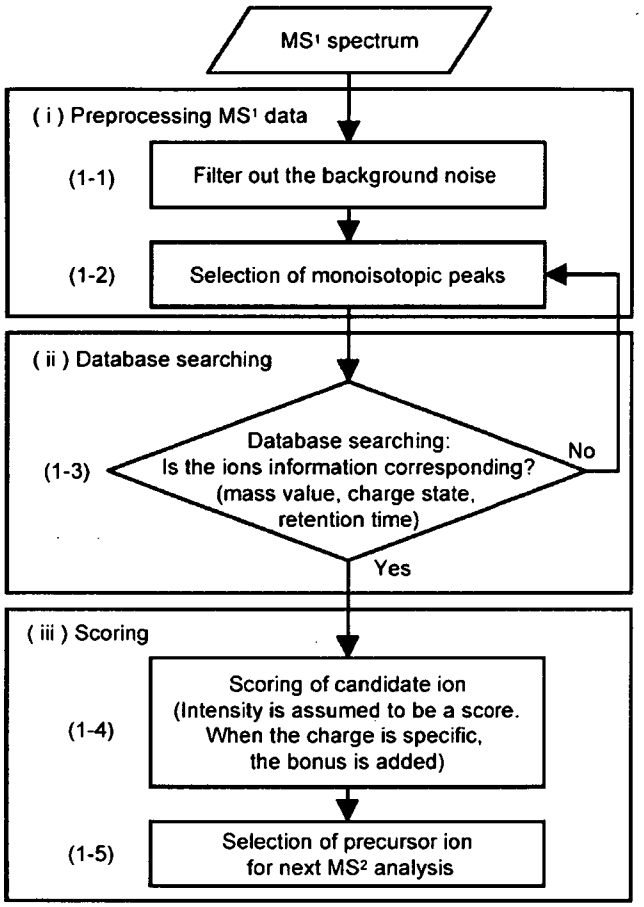

Figure 2. The processing flow of IBA (I).

user wants to give priority to a specific charge state, the parameter can be set beforehand. Finally, IBA selects the precursor ion for MS^2 analysis based on the score (1-5).

The processing time needed for the above-mentioned functions is less than 10 ms, which is the setup time of the next MS^2 acquisition. As reference data to judge whether or not the detected ions are identified with those previously selected as MS^2 precursor ions, using only mass value and charge state is insufficient. Retention time is also a very powerful reference data value to avoid repeating MS^2 on the same ion. Therefore, our system can refer to *m*, *z* and RT in a real-time manner so as to efficiently select low-abundance ions as MS^2 precursor ions. In standard techniques, such as Dynamic Exclusion™, MS^2 analysis of the same target is only allowed during a fixed time. In IBA (I), repetition of the same MS^2 analysis for the same precursor ion is allowed until the summation of intensity of the precursor ion becomes more than a definite value through all the analysis. As a result, a low-abundance ion can be analyzed microscopically more than a high-abundance ion.

We use the stored data of the DB after the Nth LC/MS run for the (N + 1)th LC/MS run. The processing time needed for this function is less than 10 ms, which is the setup time of the next MS^2 acquisition.

Auto MS^3 analysis (IBA (II))

When the MS^2 of a peptide gives insufficient fragment ion peaks, it might exhibit more fragmentation with MS^3. In order to judge the necessity of MS^3, it is essential to promptly figure out whether or not the current MS^2 data have sufficient information for identifying the peptide. The main feature of this step is to obtain the number of amino acid residues N_{aa} that can be interpreted from the MS^2 spectrum within 10 ms by concurrent assignment of b- and y-series ions to the observed peaks. The number of interpreted amino acid residues was previously considered as the criterion number N_c, which is used to judge whether the MS^2 data have sufficient information to identify the peptide. Based on this result, MS^3 could be conducted only when the number of the interpreted amino acids is below thr criterion number. In this study, we set the criterion number N_c to five.

Figure 3 shows the processing flow of IBA (II). The approach taken in IBA (II) can be broken down into four steps: (2-1) preprocessing, (2-2) candidate computation, (2-3) judgment of necessity of MS^3 analysis, and (2-4) selection of optimal precursor ion for MS^3 analysis.

(2-1) The first step is almost the same as the processing done with IBA (I). This involves a new method for noise filtering, peak centering, as well as deconvolution of the multiply charged species to singly charged ions for the raw MS^2 spectrum. This step is also very important for the interpretation of the MS^2 spectrum in IBA (II). The optimal preprocessing of data is an important step for the *de novo* sequencing using the MS^2 spectrum.

(2-2) The second step, candidate computation, is the critical step for predicting the amino acid sequences for a given computed precursor ion mass value. For this computation, a, b, c, x, y, z, the dehydration, and the deammonia peaks are considered. The basic assumption of our model is the evaluation of the intervals among all the peaks. For each interval value M, this new algorithm first computes the reward that a y (or b) ion has mass value M. If there is an interval close to M, the reward is equal to the logarithmic abundance of the peak, multiplied by a factor reflecting the co-existence of the derivative ion, such as x, z, y-18 (H_2O) and y-17 (NH_3) ions. The factor is used in the experimental detection probability when the dissociation technique is assumed to be collision-induced dissociation (CID) as reported by Fernandez-de-Cossio *et al.*[14] If the interval is not close to M, it is not used to predict the sequence. Next, the amino acid sequences are interpreted from the mass values of the precursor ions one by one by using only the peak with the corresponding mass value of the amino acid residues. This time, IBA (II) is simultaneously interpreted from the N- and C-termini to accelerate the processing.

(2-3) In the third step, the necessity of MS^3 analysis is judged from the number of interpreted amino acid residues (N_{aa}) with high scores from the predicted amino acid sequence. IBA (II) judges the necessity of MS^3 analysis from N_{aa}, which is a criterion parameter set by the user beforehand. If N_{aa} is greater than or equal to the criterion, IBA (II) judges that MS^3 analysis is not necessary and cancels the step ($N_{aa} \geq N_c$: case 1). In the case of angiotensin III (RVYIHPF, 1+), which gave sufficient peaks for sequencing, seven amino acid residues were predicted with a high score by IBA (II). In this case, the IBA will proceed to MS or MS^2 for other ion species. Meanwhile, if N_{aa} is less than the criterion, IBA (II) judges the MS^2 spectrum has insufficient information to accurately identify the correct peptide ($N_{aa} < N_c$: case 2). In

DOI: 10.1002/rcm

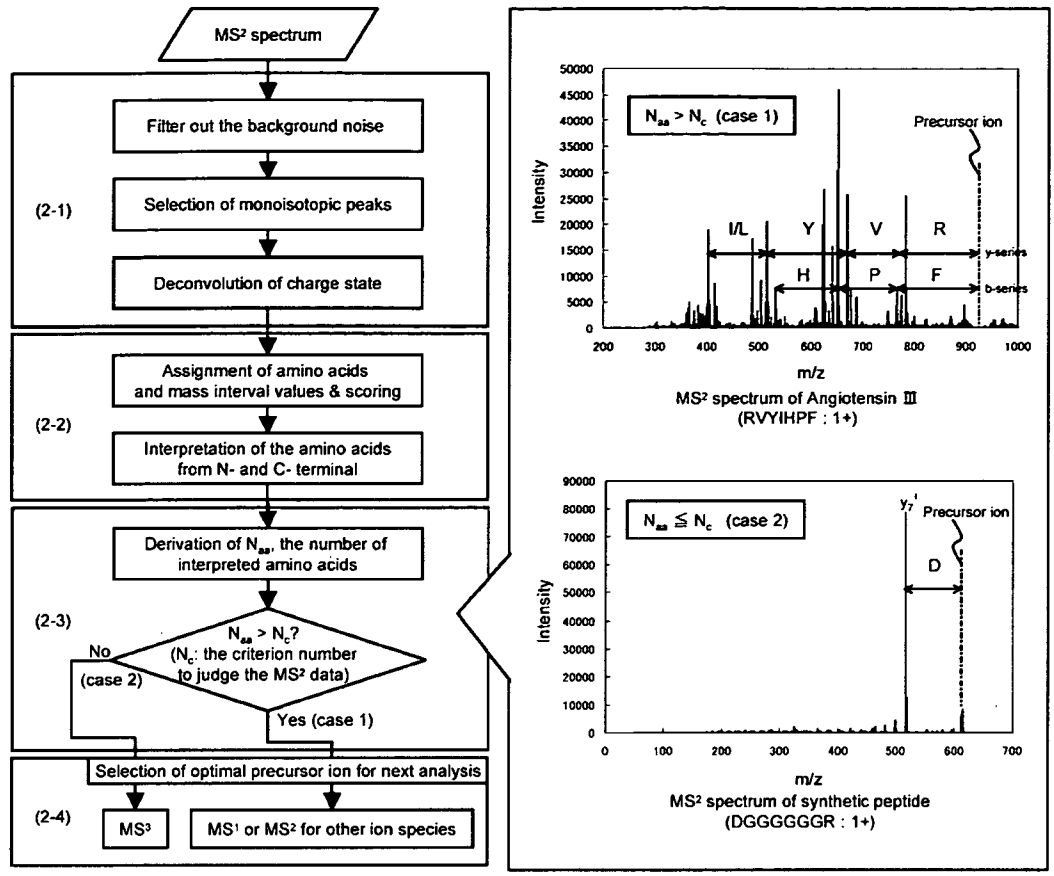

Figure 3. The processing flow of IBA (II).

the case of the synthetic peptide (DGGGGGGR, 1+), which gave insufficient peaks for sequencing, only asparatic acid (D) was predicted with a relevant score by IBA (II). In this case, the IBA will switch over to MS^3.

(2-4) Finally, if the N_{aa} is less than the criterion (case 2), IBA (II) automatically selects the precursor ion for MS^3 analysis. When the MS^3 analysis is executed, the y-ion is selected in this technique among the presumed peaks including the amino acid or the area where the score is low and uncertain by priority as a precursor ion of MS^3 analysis. This is because arginine (R) and lysine (K) of the basic amino acid residues that easily trap the proton ion added to the peptide are located in the C-terminus when the protein is digested by trypsin, and the possibility that the y-ion is detected with high intensity is high. Figure 4 shows the MS^3 spectrum of the y_7^+ ion of the synthetic peptide (DGGGGGGR) which was selected as a MS^3 precursor ion by IBA (II). By performing the MS^3 analyses to the y_7^+ ion, six amino acid residues (DGGGGG) of DGGGGGGR could be interpreted with high scores. Thus, some peptides will be identified by the auto MS^3 function.

Thus, IBA (II) is carried out on the obtained MS^2 spectrum and the MS^3 analysis is executed for accurate peptide identification when the number of interpreted amino acid residues in the MS^2 spectrum is less than the criterion which is set beforehand.

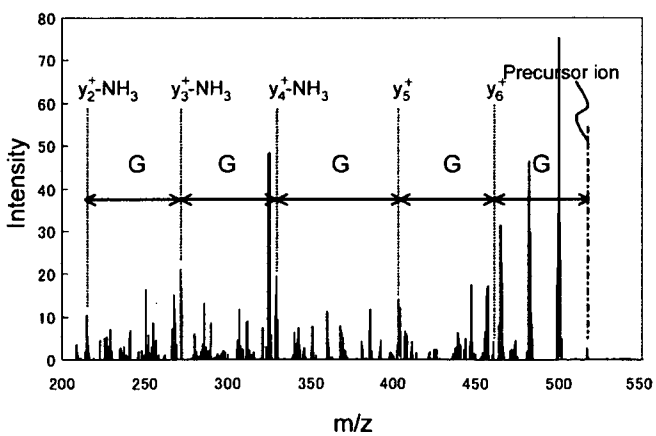

Figure 4. An example of the judgment of IBA (II).

EXPERIMENTAL

In order to achieve real-time optimization of tandem mass spectrometry, IBA was installed in a modified prototype model of a nanoLC/ion-trap/oaTOF mass spectrometer equipped with an electrospray ionization source (ESI) (Hitachi High-Technologies, Ltd., Tokyo, Japan).

We tested our technique by repeatedly analyzing a tryptic digest of soluble proteins extracted from *Saccharomyces cerevisiae* S288C, a typical crude sample. Since the nanoLC pump system is a non-split type, the retention time for detected ions is reproducible. The mobile phase A was water with 0.1% formic acid and B was a solution of 98% acetonitrile with 0.1% formic acid. A 180-min gradient was performed from 2% to 50% of mobile phase B at an effluent flow rate of 50 nL/min.

DOI: 10.1002/rcm

The sample was injected with an injection valve (M485, Upchurch Scientific, WA, USA) and was separated with a 600-mm-long monolithic column with a diameter of 30 mm (Kyoto Monotech, Kyoto, Japan). The backpressure of the nanoLC pump was about 5 MPa. A high voltage of 1.4 kV was applied to a fused-silica capillary spray chip with a diameter of 5 μm (New Objective, MA, USA) and the sampling orifice of the mass spectrometer was heated with a heater to 140°C.

In a preliminary LC/MS run, a few of the most intense ions detected in every MS spectrum are selected as precursors for MS^2, and their masses, charges, and retention times are automatically registered in an internal database. In the next run, the same sample as that used in the first run is analyzed using the database. The ions registered in the database are then excluded from the precursor-ion selection to avoid duplicating the analysis. With a repetition of such LC/MS runs, the number of ions registered in the database becomes significant, so low-abundance ions are readily analyzed. On the other hand, real-time *de novo* sequencing analysis is performed just after obtaining an MS^2 spectrum, and an MS^3 spectrum is obtained for accurate peptide identification only when the number of interpreted amino acids in the MS^2 spectrum is fewer than five.

Protein identification

The MS^2 identification was performed by protein database searching used by the Mascot® program[1] for all MS^2 and MS^3 spectra. The obtained MS^3 spectra were merged with the MS^2 spectra, which include precursor ions of MS^3 spectra. The database of *Saccharomyces cerevisiae* S288C (6332 sequences) was obtained from the Genome Information Broker (GIB), which is based on the data from the National Center for Biotechnology Information. Protein identifications are based on peptide identifications that have Mascot ion scores that correspond to at least a 95% probability of being correct.

RESULTS AND DISCUSSION

The information of the analyzed precursor that had been obtained from LC/MS analysis was automatically stored in an internal database, and used in the following LC/MS analysis.

Figure 5 indicates the time which was required to analyze each MS or MS^2 spectrum. The MS^1 spectrum required from 2 to 5 ms to optimize the next analysis. For the MS^2 spectrum, all processing was completed within about 2 ms. The processing time is within about 5 ms of the range of the retention time (from 30 to 100 min) when many ion species are detected. It is shown that on-line data-dependent MS^n ($n = 2, 3$) could be feasible and there is no negative influence on the throughput of the analysis.

Figures 6 and 7 show the effects of IBA (I). Figure 6 shows the distribution of the ionic species stored in an internal database. Almost 2000 kinds of different (mass value or charge state or retention time) ionic species were selected as MS^2 precursor ions and stored in an internal database in each LC/MS run. By repeating the same LC/MS run five times, 9078 kinds of different ion species were stored in total. Thus, by avoiding duplicate MS^2 analyses using IBA (I), the low-abundance peptides could be selected efficiently as MS^2 precursor ions.

Figure 7 shows the total number of identified proteins. To confirm the effect of a function of IBA (I), the result of the measurement without using an internal database is shown as auto MS/MS. The number of identified proteins increases almost linearly by a function of IBA (I), which selects different MS^2 precursor ions in each LC/MS run. In the first LC/MS run, 162 kinds of proteins were identified. On the other hand, 533 kinds of proteins were identified by repetition of the same LC/MS run five times. Thus, the number of proteins identified by running the analysis five times increases by 3.3 times the number of proteins identified in the first LC/MS run. On the other hand, in the case of auto MS/MS, the number of identified proteins hardly increases after the third run. It is cause to analyze the same precursor ion which is in high abundance repeatedly. Therefore, the effective analysis of low-abundance proteins such as those related to disease could be performed by repeating an LC/MS analysis with IBA (I).

The MS^3 analysis supplies the information of the peptide sequence, but lowers the total throughput. So, in this study, we set the conditions for running MS^3 analysis strictly; that

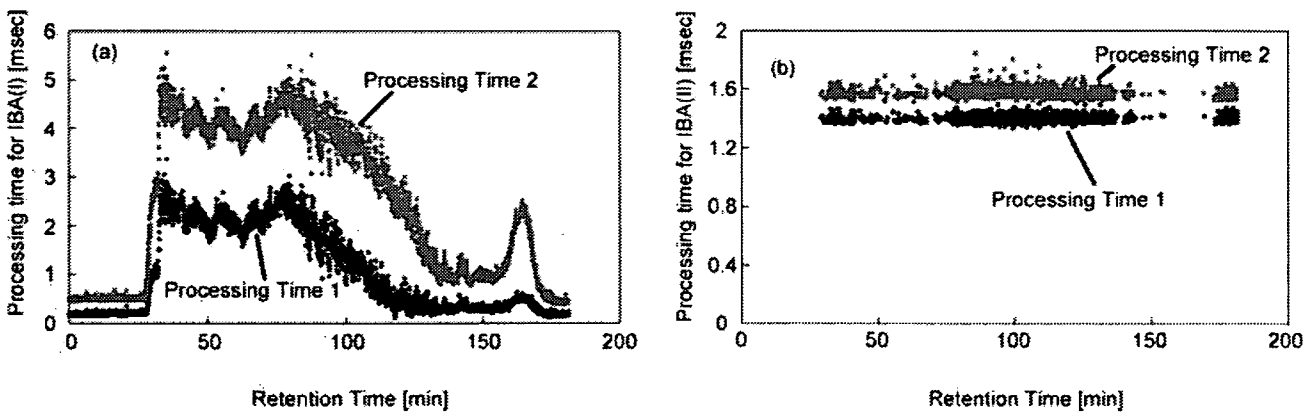

Figure 5. Processing time for real-time optimization. (a) IBA (I): Processing Time 1: time from noise filtering to peak detection, Processing Time 2: time from noise filtering, peak detection, inside database searching and selection of MS^2 precursor ion. (b) IBA (II): Processing Time 1: time from noise filtering to peak detection, Processing Time 2: time from noise filtering, peak detection, *de novo* sequencing and judgment of necessity of MS^3 analysis.

DOI: 10.1002/rcm

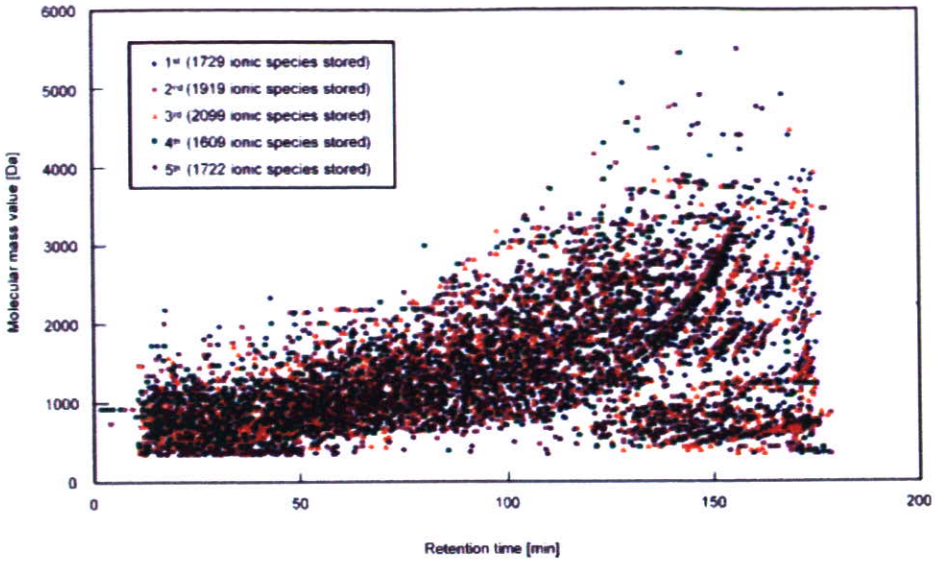

Figure 6. The precursor ions (molecular masses vs. retention times) selected by IBA (I) (5 cycles)

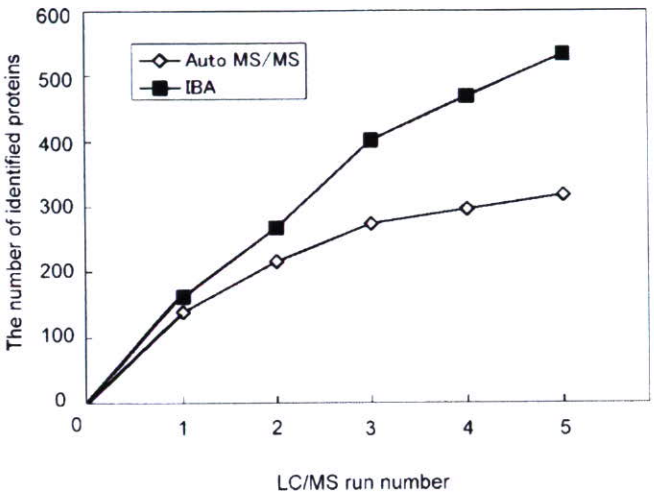

Figure 7. The number of identified proteins. Comparison of the number of identified proteins between IBA and auto MS/MS.

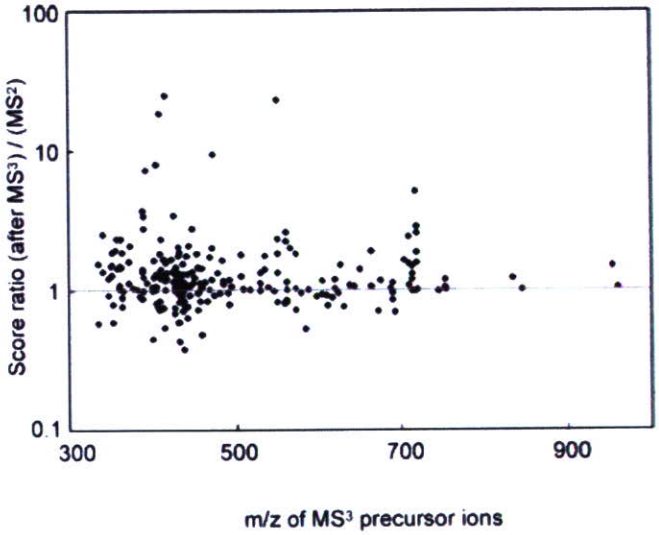

Figure 8. The score ratio (after MS^3/MS^2) of ion scores.

is, the threshold value of intensity of precursor ion to execute MS^3 analysis was set high. As a result, the frequency of MS^3 analysis depended on the LC/MS run and the ratio of the MS^3 analysis was from about 3 to 10% of the MS^2 analysis. Figure 8 shows the ratio of the Mascot® score of merged spectrum MS^2 with MS^3 to score of MS^2 spectrum. If the ratio is greater than 1.0, the identification accuracy has improved by the auto MS^3 analysis. In Figure 8, it was confirmed that peptide ion score was improved by the auto MS^3 analysis with 70% of the cases which executed MS^3. On the other hand, it was confirmed that the ratio was lower than 1.0 with 30% of the cases which performed MS^3. Figures 9 and 10 show typical examples of each case. In the case where the score of peptide improves, i.e. the ratio was greater than 1.0, it can be confirmed that the information on the amino acid sequence is supplemented by performing the MS^3 analysis to the y_{13}^{++} ion, as shown in Fig. 9. The improvement in the score is due to the increasing of the number of assigned fragment peaks with the auto MS^3 analysis.

On the other hand, Fig. 10 shows an example of the case where the score of the peptide decreases. In Fig. 10, the candidate peptide sequence at the 1st place has changed from DATKRR to DADGKLK with decreasing score. It is considered that the score has decreased because the candidate sequence DATKRR was a false-positive sequence. In the algorithm of Mascot®, the existence of unassigned peaks decreases the score. Therefore, in 30% of the cases which executed MS^3, it is considered that the score has decreased by the exclusion of the false-positive sequence and the identification accuracy of the protein improves by the exclusion of the false-positive candidates.

DOI: 10.1002/rcm

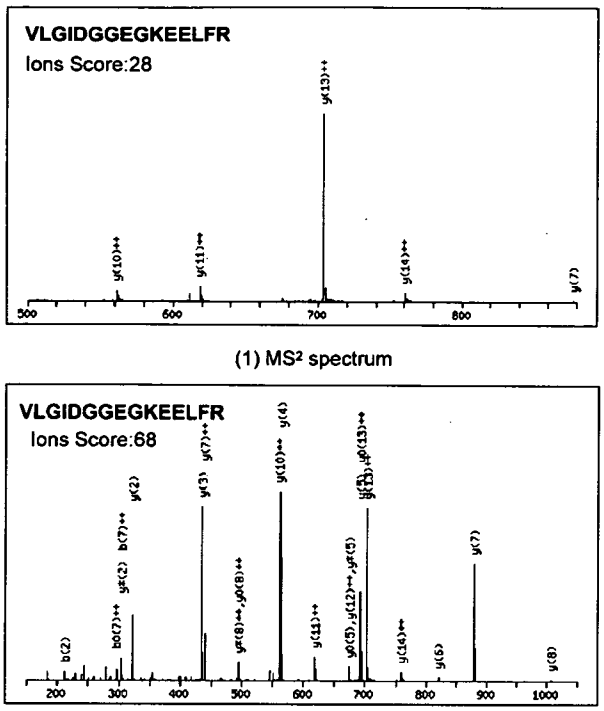

(1) MS² spectrum

(2) MS² and MS³ spectrum

Figure 9. Example of analyzing MS^3.

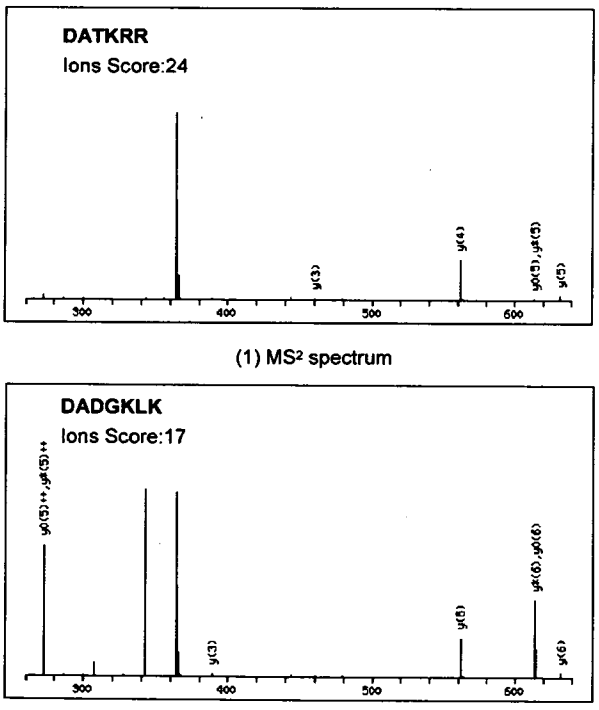

(1) MS² spectrum

(2) MS² and MS³ spectrum

Figure 10. Example of analyzing MS^3.

Furthermore, in the case where the score decreases though volume of information has obviously increased with auto MS^3 analysis, there is a possibility that the amino acid sequence was modified posttranslationally or not registered in the protein database. For these cases, the change of the database searching condition or analysis using *de novo* sequencing is effective.

CONCLUSIONS

We have installed the software, based on our method, on a modified prototype model of a nanoLC/ion-Trap/oaTOF mass spectrometer equipped with an ESI source. We applied it to a high-protein mixture as a target sample and checked the fundamental functions from the results. The following results were obtained.

- The total processing time to evaluate raw MS and raw MS^2 data for optimization by tandem mass spectrometry is less than 10 ms, which is the setup time of the next MS^2 acquisition.
- The charge states of 90% of precursor ions are correctly identified in real time by this method.
- The total number of identified proteins in five runs was higher by a factor of 3.3 compared to that in the first run.
- The ion scores for peptide identification increase significantly in about 70% of cases when the MS^3 spectra, combined with MS^2 spectra before being subjected to Mascot® analysis, are used.

Therefore, the real-time optimization technique for tandem mass spectrometry is feasible and useful to detect low-abundance proteins with high throughput and high accuracy in highly complex protein mixtures.

Acknowledgement

We thank Dr. Yoshiya Oda of Eisai Co., Ltd. for fruitful discussions. We also acknowledge Naomi Manri and Masako Ishimaru for their invaluable assistance with these experiments and the financial support provided by Hitachi High Technologies, Ltd. This work was supported by the New Energy and Industrial Technology Development Organization (NEDO), Japan.

REFERENCES

1. Perkins DN, Pappin DJC, Creasy DM, Cottrell JS. *Electrophoresis* 1999; **20**: 3551.
2. Eng JK, McCormack AL, Yates JR III. *J. Am. Soc. Mass Spectrom.* 1994; **5**: 976.
3. Biemann K, Martin SA. *Mass Spectrom. Rev.* 1987; **6**: 1.
4. McCormack AL, Somogyi A, Dongre AR, Wysocki VH. *Anal. Chem.* 1993; **65**: 2859.
5. Wysocki VH, Tsaprailis G, Smith LL, Breci LA. *J. Mass Spectrom.* 2000; **35**: 1399.
6. Tabb DL, Huang Y, Wysocki VH, Yates JR III. *Anal. Chem.* 2004; **76**: 1243.
7. Cu C, Somogyi A, Wysocki VH, Medzihradszky KF. *Anal. Chim. Acta* 1999; **397**: 247.
8. Kapp EA, Schutz F, Reid GE, Eddes JS, Moritz RL, O'Hair RAJ, Speed TP, Simpson RJ. *Anal. Chem.* 2003; **75**: 6251.
9. Mohammed S, Chalmers MJ, Gielbert J, Ferro M, Gora L, Smith DC, Gaskell SJ. *J. Mass Spectrom.* 2001; **26**: 1260.
10. Mann M, Wilm M. *Anal. Chem.* 1994; **66**: 4390.
11. Horn DM, Zubarev RA, McLafferty FW. *Proc. Natl. Acad. Sci.* 2000; **97**: 10313.
12. Searle BC, Dasari S, Turner M, Reddy AP, Choi D, Wilmarth PA, McCormack AL, David LL, Nagalla SR. *Anal. Chem.* 2004; **76**: 2220.
13. Shevchenko A, Ghernushevich I, Ens W, Standing KG, Thomson B, Wilm M, Mann M. *Rapid Commun. Mass Spectrom.* 1997; **11**: 1015.
14. Fernandez-de-Cossio J, Gonzalez J, Betancourt L, Besada V, Padron G, Shimonishi Y, Takao T. *Rapid Commun. Mass Spectrom.* 1998; **12**: 1867.

DOI: 10.1002/rcm

FEBS Letters 580 (2006) 199–205

Evidence for phosphorylation of rat liver glucose-regulated protein 58, GRP58/ERp57/ER-60, induced by fasting and leptin

Kanako Kita, Nobuaki Okumura, Toshifumi Takao, Makoto Watanabe, Toshiya Matsubara, Osamu Nishimura, Katsuya Nagai*

Laboratory of Proteins Involved in Homeostatic Integration, Institute for Protein Research, Osaka University, 3-2, Yamada-Oka, Suita, Osaka 565-0871, Japan

Received 8 November 2005; revised 28 November 2005; accepted 29 November 2005

Available online 9 December 2005

Edited by Gianni Cesareni

Abstract Glucose-regulated protein 58 (GRP58)-like immunoreactivity in rat liver obtained in the evening or after fasting underwent an electrophoretic band-shift, which disappeared after phosphatase-treatment. Since mass spectrometric analysis raised a possibility that Ser150 of GRP58 is phosphorylated, an antibody against the phosphoserine150 GRP58 was generated. Immunoreactivity to this antibody was increased in the evening and after fasting. Since GRP58 was shown to interact with signal transducer and activator of transduction 3 (STAT3), a leptin-related protein, the effect of leptin was examined. Immunoreactivity to the anti-phosphoGRP58 antibody was markedly elevated after the leptin injection, indicating that Ser150 of GRP58 is phosphorylated after fasting and leptin-treatment.

Keywords: GRP58; ERp57; MALDI-TOF-MS; Alkaline phosphatase; Hydrogen fluoride; Fasting; STAT3; Phosphorylation

1. Introduction

To investigate daily changes in liver function, protein expression patterns in the rat liver were analyzed by proteome analysis using one- and two-dimensional electrophoresis (1DE and 2DE), mass spectrometry and immunoblotting. Multiple spots of immunoreactivity to an anti-glucose-regulated protein 58 (GRP58) antibody were detected. GRP58 is a stress protein of about 60 k whose expression is induced in conditions such as in glucose starvation and viral infection [1,2]. It is homologous to protein disulfide isomerase (PDI) and possesses two thioredoxin domains including an active motif (CGHC) of the disulfide redox response as well as PDI [3]. Recently, it was reported that GRP58 modulates the intracellular signal transduction by interacting with signal transducer and activator of transduction 3 (STAT3) [4], a leptin-related protein, and coexists with cytoplasmic STAT3 and the plasma membrane complexes [5,6]. The aim of this study was determine whether the multiple spots of GRP58-like immunoreactivity were caused by its phosphorylation and how starvation and leptin affected on the patterning of these spots. It was found that serine150 of GRP58 is phosphorylated by fasting and or treatment with leptin.

*Corresponding author. Fax: +81 6 6879 8633.
E-mail address: k_nagai@protein.osaka-u.ac.jp (K. Nagai).

Abbreviations: 1DE, one-dimensional electrophoresis; 2DE, two-dimensional electrophoresis; GRP58, glucose-regulated protein 58; PDI, protein disulfide isomerase; STAT, signal transducer and activator of transduction; ZT, zeitgeber time; SDS–PAGE, SDS–polyacrylamide gel electrophoresis; aCSF, artificial cerebrospinal fluid; LCV, lateral cerebral ventricle

2. Materials and methods

2.1. Animals and liver sampling

Male Wistar strain rats, weighing 250–300 g, were used. They were housed in a room illuminated for 12 h (lights on 07:00–19:00 h) and kept at 24 ± 1 °C for at least 2 weeks before the experiments. Food (type ME, Oriental Yeast Co., Tokyo) and water were freely available. Animal care and handling were approved by the Institutional Animal Care and Use Committee of Osaka University. Animals were sacrificed by decapitation at 12:00 h [Zeitgeber time (ZT) 5], 18:00 h (ZT11), 24:00 h (ZT17) and 06:00 h (ZT23) and livers were obtained. ZT represents hours after the light turned on under a 12-h light/12-h dark cycle [7].

To determine the effect of fasting, rats were deprived of food and sacrificed at 12, 24, 36 and 48 h after which their livers were harvested and analyzed.

2.2. Two-dimensional gel electrophoresis

Immobilized pH gradient (IPG) gel strips (pH 4–7; NL, 7, 13 and18 cm; Amersham–Pharmacia Biotech) were used as the first dimension gel of 2DE for isoelectric focusing. Liver samples were homogenized in ten volumes of 8 M urea, 60 mM DTT, 2% Chaps, and 10 mM Tris–HCl (pH 7.4), and when examined with protein staining 200 μg of protein was applied on an 18 cm gel strip and examined with mass spectrophotometry. The samples were mixed with 150 μl (for 7 cm gels) or 280 μl (for 13 cm gels) of rehydration buffer containing 7 M urea, 2 M thiourea, 2% Chaps, 10 mM DTT, 2 mM Tris (2-cyanoethyl) phosphine, 2% pharmalyte 3–10, and a trace amount of bromophenol blue, and the gels rehydrated. Isoelectric focusing was then carried out on the gel strips using an electrophoretic apparatus where the voltage was increased stepwise to 4500 V for 18 cm followed by incubation at each voltage for 4–5 h. After the first dimensional electrophoresis, the strips were incubated three times with 5 ml of a solution containing 50 mM Tris–HCl (pH 6.8), 8 M urea, 2% (w/v) SDS, and 60 mM DTT for 30 min, and once with 5 ml of solution containing 50 mM Tris–HCl (pH 6.8), 8 M urea, 2 M thiourea, 20 mM DTT, 30% (w/v) glycerol, 2% (w/v) SDS, and 2 mM Tris(2-cyanoethyl)phosphine for 30 min. In the second dimensional electrophoresis, SDS–polyacrylamide gels (9–16% T/2.6% C) without a stacking gel were used as resolving gels.

2.3. Protein staining and image analysis

After the 2DE, gels were washed for 30 min in a gel fixing solution containing 7% acetic acid and 10% methanol. For maximum sensitivity all gels were stained using SYPRORuby protein gel fluorescent stain

0014-5793/$32.00
doi:10.1016/j.febslet.2005.11.074

(BioRad) for 3 h and rinsed in fixing solution for 60 min. Fluorescent signals were detected using a fluorescence image analyzer (Fluorimager 595; Molecular Dynamics).

2.4. 1D-PAGE and 2D-PAGE for Western blotting for analysis of GRP58

For 1D-PAGE, an equal amount of protein from each sample (10 μg) was electrophoresed on an 8% SDS–polyacrylamide gel. For the first dimension of 2D-PAGE, IPG gel strips (pH 4–7; NL, 7 and 13 cm) were used. The sample was mixed with rehydration buffer and applied on a gel (60 μg protein for a 7 cm gel and 100 μg for a 13 cm gel). The voltage for the electrophoresis was increased stepwise to 3000 V at 100 μA intervals for 3–5 h.

After samples were separated by either 1D-PAGE or 2D-PAGE, they were transferred onto a nitrocellulose membrane (Schleicher & Schuell). The membranes were blocked in Tris-buffered saline (pH 7.4) containing 0.1% Tween 20 (Tween-TBS), incubated with rabbit anti-GRP58 polyclonal antibodies (StressGen Biotechnologies) for 3 h, washed with Tween-TBS, incubated with HRP conjugated secondary antibodies (Cell Signaling Technology) against rabbit IgG for 1 h, and washed with Tween-TBS. Immunoreactivity to the anti-GRP58 antibodies was visualized using an enhanced chemiluminescence system (NEN Life Science Products).

2.5. MALDI-TOF-mass spectrometry

Gel sections from the 2-DE gels were incubated with 1 ml of 50 mM ammonium bicarbonate-50% methanol at 37 °C overnight. The solution was then removed and the gel sections incubated in a solution containing 100 μl of 10 mM DTT-100 mM ammonium bicarbonate for 60 min at 60 °C. The gels were alkylated with 100 μl of 50 mM iodoacetamide/50 mM ammonium bicarbonate for 30 min at room temperature. The gels were washed twice with distilled water and dried under a vacuum pump. The gels were then digested with 50 μl of 50 mM ammonium bicarbonate containing 10% acetonitrile and 1 pmol of trypsin (Sigma) for 16 h at 37 °C and resultant peptides eluted in a solution containing 50% acetonitrile, 50 mM ammonium bicarbonate, and 0.1% TFA. The supernatant obtained after centrifugation was concentrated to a volume below 30 μl under vacuum and desalted with ZipTip 18 (Millipore). For measurement of mass spectrometry (MS) spectra, 0.5 μl of sample solution was mixed with 0.5 μl of matrix solution containing 10 mg/ml α-cyano-4-hydroxycinnamic acid (CHCA), deposited on the target, and dried completely. MALDI-TOF-mass spectra were generated using an AXIMA-CFR instrument (Shimadzu Corp., Japan) under reflectron mode operating conditions after calibration using ACTH and bradykinin. Peptides were matched using the MASCOT database search under the following conditions: fixed modifications of carbamidomethyl (C); variable modifications of phosphorylated Ser and Thr; Taxonomy of Rattus; and a tolerance of one missed cleavage.

2.6. Alkaline phosphatase treatment

Sample was incubated with 0.5 μl alkaline phosphatase (New England BioLab) for 12 h at 4 °C. Then the sample was separated with SDS–PAGE, and immunoblotted using anti-GRP58 antibodies.

2.7. Leptin injection

For intracranial administration of leptin, a brain cannula, made of PE-10 (Clay Adams, Parsippany, NJ), was inserted into the right lateral cerebral ventricle (LCV), three days before the experiment under pentobarbital anesthesia (35 mg/kg) as previously described [8]. The effect of leptin on GRP58 was examined by injecting leptin [Sigma–Aldrich, 10 μg/20 μl of artificial cerebrospinal fluid (aCSF)] into the LCV at each time point under unanesthetic condition using the LCV cannula. For control experiment, 20 μl of aCSF was injected into the LCV. Animals were sacrificed at 0, 15, 30, 60, and 180 min after the administration of leptin or aCSF and liver samples were obtained.

2.8. Anti-phosphorylated GRP58 Ser-150 antibody production

A synthetic peptide, EFKKFIpSDKDASC (corresponding to amino acid residues of GRP58 surrounding Ser150) was conjugated with Imject Maleimide activated mcKLH (Pierce), mixed with Freund's complete adjuvant and injected into rabbits. The resultant polyclonal antiserum against this peptide was subjected to affinity purification and used to detect GRP58 phosphorylated on Ser150.

2.9. Dephosphorylation of proteins using hydrogen fluoride–pyridine

Dephosphorylation of proteins using hydrogen fluoride–pyridine was performed as described previously [9]. Samples were dephosphorylated using hydrogen fluoride–pyridine, neutralized with NaOH, desalinated by using a centrifugal filter (Millipore), then eluted in TNE buffer.

2.10. Immunoprecipitations

Protein samples were pre-treated with protein G–Sepharose (Amersham-Pharmacia Biotech) for 1 h at 4 °C. After centrifugation, the supernatant was incubated for 1 h at 4 °C with protein G–Sepharose that had been preincubated with 2 μg of mouse anti-Stat3 antibody (BD Biosciences Pharmingen) or mouse IgG. The Sepharose beads were washed five times with TNE buffer. Immunoprecipitated proteins were analyzed using SDS–PAGE electrophoresis.

3. Results

3.1. GRP58 identified as a protein showing daily changes in its expression in rat liver

To identify proteins showing daily changes in their expression in the rat liver, livers were sampled at 18:00 h (ZT11) and 06:00 h (ZT23) and their proteins were separated by 2DE after homogenization. The 2DE-gels were stained with SYPRO Ruby and about 1200 spots were detected in gels of pH 4–7 after a comparative analysis of the protein patterns was carried out using the image analysis software, PDQUEST. Among the proteins that showed changes in their expression patterns, a spot (shown as arrow heads in Fig. 1A) was identified that appeared to undergo daily changes in its expression pattern (high at ZT11 and low at ZT23) after quantitative analysis. Peptide mass fingerprinting of 21 fragments generated from the spot showed that they matched the amino acid sequence of GRP58 with a MASCOT score of 243, and a sequence coverage of 39%, indicating that this protein is GRP58 (Table 1).

3.2. Confirmation of the protein as GRP58

To confirm that the above protein spot is actually GRP58, livers were sampled at ZT 5, 11, 17, and 23, examined by SDS–PAGE and immunoblotted using a rabbit anti-GRP58 polyclonal antibodies. However, a clear daily change in the immunoreactivity to the anti-GRP58 antibodies was not detected in 1DE (Fig. 1B), even though a clear shift in the migration of the immunoreactive band was observed at ZT11 in comparison with sample bands obtained at other time points (Fig. 1B). These results suggested that this protein might undergo protein modification such as phosphorylation. The protein was examined further using 2DE and immunoblotting with the anti-GRP58 antibodies which detected four immunoreactive spots of similar molecular sizes but with different isoelectric points (1-1, 1-2, 1-3 and 1-4 in Fig. 1C). The spot identified in Fig. 1A (arrowheads) was identical to the spot at 1-3 in Fig. 1C. Immunoreactivities of the GRP58-like immunoreactive substance (GRP58LIS) at more acidic isoelectric points (1-3 and 1-4) increased at ZT11 in comparison to those at other time points (Fig. 1C).

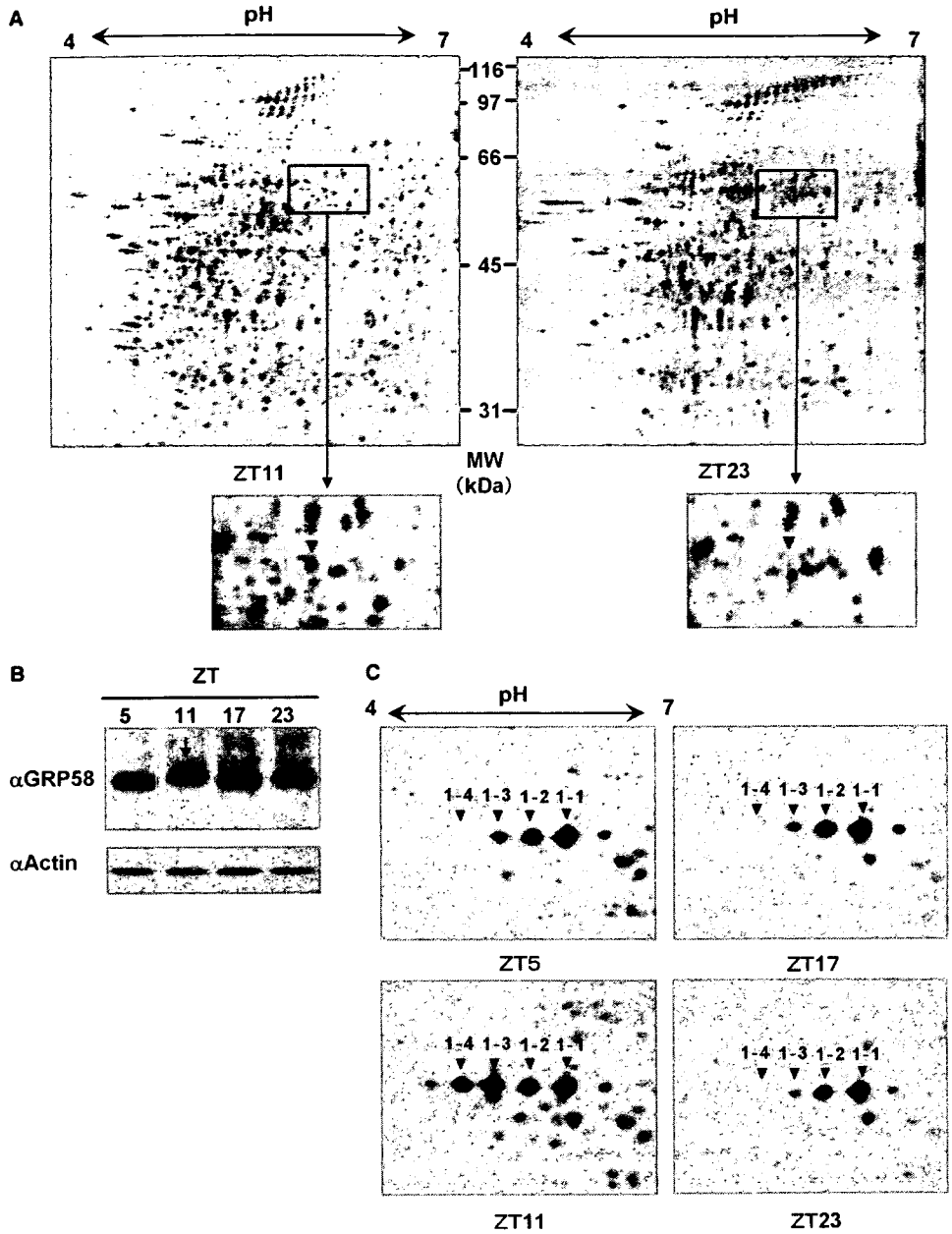

Fig. 1. Detections of proteins exhibiting daily expression changes in the liver. (A) 2DE of rat liver was sampled at ZT11 and ZT23 with isoelectric focusing showed different expression patterns for spot showed by arrowheads. (B) Immunoblotting using an anti-GRP58 antibody in 1DE. Livers were sampled at 12:00 (ZT5), 18:00 (ZT11), 24:00 (ZT17) and 06:00 (ZT23) h under 12-h light and 12-h dark period (light on at 07:00 h). Livers were homogenized, centrifuged, and supernatants were dissolved in SDS–PAGE sample buffer. Samples then underwent electrophoresis and were immunoblotted using anti-GRP58 antibodies. (C) Immunoblotting using an anti-GRP58 antibodies in 2DE. Different expression patterns were observed spots 1-1, 1-2, 1-3 and 1-4.

3.3. Phosphorylation of GRP58

Since horizontal movement of the protein spots in the 2DE is often observed due to changes in isoelectric point induced by protein phosphorylation, the result obtained in the experiment shown in Fig. 1C raised the possibility that phosphorylation of GRP58 might be increased at ZT11. To examine whether GRP58 was phosphorylated at ZT11, the liver sample obtained at ZT11 was treated with alkaline phosphatase and examined by immunoblotting. As seen in Fig. 2, after treatment with phosphatase, the mobility of GRP58LIS at ZT11 slightly increased in 1DE (Fig. 2A) and the immunoreactivities of 2 spots in the more acidic side (1-3 and 1-4) decreased while the immunoreactivity of the spot at the most alkaline side (1-1) increased at ZT11 in 2DE gel (Fig. 2B). These findings suggest that GRP58 is phosphorylated at ZT11.

3.4. Effects of fasting

Since protein expression in the liver is known to be frequently affected by fasting and ZT11 is almost at the end of the resting (non-eating) period for nocturnal animals like rats, it was hypothesized that the above daily change in GRP58 mobility might be affected by fasting. Therefore, liver samples

Table 1
Mascot search results for fragments of protein spots corresponding to GRP58

Signal	Observed	Mr(expt)	Mr(calc)	Delta	Miss	Start-end	Sequence	Spot no.			
1	1191.70	1190.69	1190.59	0.10	0	63–73	LAPEYEAAATR	1-1	1-2	1-3	1-4
2	1397.81	1396.80	1396.57	0.23	0	83–94	VDCTAVTNTCNK	1-1	1-2	1-3	1-4
3	1652.88	1651.87	1651.76	0.11	1	105–119	IFRDGEEAGAYDGPR	1-1	1-2	1-3	1-4
4	817.48	816.47	816.38	0.09	1	147–152	KFIpSDK			1-3	1-4
5	1587.91	1586.90	1586.81	0.09	1	148–161	FISDKDASVVGFFR	1-1	1-2		
6	1394.75	1393.74	1393.65	0.09	0	162–173	DLFSDGHSEFLK	1-1	1-2	1-3	
7	1607.83	1606.82	1606.74	0.08	0	259–271	DLLTAYYDVDYEK	1-1	1-2	1-3	1-4
8	1951.01	1950.00	1949.93	0.08	1	259–274	DLLTAYYDVDYEKNTK			1-3	
9	782.38	781.37	781.35	0.02	0	275–280	GSNYWR	1-1	1-2	1-3	1-4
10	1747.05	1746.04	1745.92	0.12	1	289–304	TFLDAGHKLNFAVASR	1-1	1-2	1-3	1-4
11	877.52	876.51	876.48	0.03	0	297–304	LNFAVASR	1-1	1-2	1-3	1-4
12	2733.30	2732.29	2732.40	−0.11	1	305–329	KTFSHELSDFGLESTTGEIPVVAIR	1-1	1-2	1-3	1-4
13	2605.24	2604.23	2604.31	−0.07	0	306–329	TFSHELSDFGLESTTGEIPWAIR	1-1	1-2	1-3	1-4
14	1172.61	1171.60	1171.53	0.07	0	336–344	FVMQEEFSR	1-1	1-2	1-3	1-4
15	1472.78	1471.77	1471.68	0.10	1	336–347	FVMQEEFSRDGK	1-1	1-2	1-3	
16	1529.89	1528.88	1528.77	0.12	1	352–363	FLQEYFDGNLKR	1 -1	1-2	1-3	1-4
17	1801.03	1800.02	1799.93	0.09	1	364–379	YLKSEPIPETNEGPVK			1-3	
18	1341.74	1340.73	1340.68	0.06	0	449–460	GFPTIYFSPANK	1-1	1-2	1-3	1-4
19	1469.86	1468.85	1468.77	0.08	1	449–461	GFPTIYFSPANKK	1-1	1-2	1-3	1-4
20	1363.76	1362.75	1362.71	0.04	0	472–482	ELNDLISYLQR				
21	1593.92	1592.91	1592.84	0.07	0	483–496	EATNPPIIQEEKPK	1-1	1-2	1-3	

MALDI-TOF-mass spectra were obtained using an AXIMA-CFR instrument (Shimadzu Corp., Japan). The MASCOT data base search identified Spot1-3 as a glucose-regulated protein of 58 kDa. Twenty-one peaks were matched to GRP58 with a score of 243 and a sequence coverage of 39%. The following conditions were used for searching the database: fixed modifications of carbamidomethyl (C); variable modifications included phosphorylated Ser and Thr; Taxonomy: Rattus; peptide tolerance: ±0.3 Da (Table 1).
Mr(expt), expected molecular mass; Mr(calc), calculated molecular mass.

were obtained from rats at 0 h and after 12, 24, 36 and 48 h of food deprivation. Mobility of GRP58LIS on 1DE gel was decreased when the liver samples were obtained after 12- and 24-h fasting in comparison to those obtained at the other time points (Fig. 2C). When these samples were analyzed on 2DE gels, it was observed that after 12- and 24-h fasting, the immunoreactivities of GRP58LIS at more acidic side (1-3 and 1-4 in Fig. 2D) were elevated but that those at 36- and 48-h of fasting were decreased (Fig. 2D). These findings indicate that phosphorylation of GRP58 in the liver is induced by fasting.

3.5. Effect of intracranial injection of leptin

Recently, it was suggested that GRP58 interacts with STAT3 to modulate intracellular signal transduction [4–6]. Since STAT3 was suggested to be involved in the intracellular signal transduction of leptin and a functional leptin receptor exists in the brain [10], the effect of intracranial injection of leptin on the mobility of GRP58 was examined. Three hours after leptin (Sigma–Aldrich, 10 μg/20 μl of a CSF) was injected into LCV using the LCV cannulae under un-anesthetic condition, the mobility of GRP58LIS from the liver was clearly shifted in 1DE (Fig. 2E) and the immunoreactivities of GRP58LIS with acidic isoelectric points (1-3 and 1-4 in Fig. 2D) increased in 2DE.

3.6. Phosphorylation site of GRP58 induced by fasting and leptin

To identify the phosphorylation site(s) of GRP58 after 12-h fasting, peptide mass finger printing was carried out on the four spots of GRP58LIS (1-1, 1-2, 1-3, 1-4 in Fig. 2D). The mass spectrometry data showed that a fragment of 1587.91 Da (sequence of GRP58 between amino acids (aa) 148–161; FISDKDASVVGFFR in Table 1) was present in spots 1-1 and 1-2 but not in spots 1-3 and 1-4. Since phosphorylated fragment was sometimes hardly detected with MALDI-TOF-MS, it was possible that this fragment was phosphorylated in spots 1-3 and 1-4. Furthermore, the molecular mass of the first half fragment (corresponding to KFISDK) was 80 Da higher than that of the calculated molecular mass of the fragment, indicating that it was phosphorylated on one of the internal serine residues, most probably serine 150. It was also possible that unphosphorylated KFISDK (736 Da) might not be detected because of the lower mass than detecting threshold MALDI-TOF-MS. In order to obtain further support for the phosphorylation of this residue after fasting and leptin injection, we conducted a search using NetPhos which allows sequence- and structure-based prediction of eukaryotic protein phosphorylation sites [11]. NetPhos predicted with strong probability that the serine residue at aa 150 of GRP58 would be phosphorylated. To test this possibility, a rabbit polyclonal antibodies against the sequence from 144 to 156 of phosphorylated GRP58 (EFKKFIpSDKDASC)-conjugated with KLH was generated. This anti-phosphoGRP58 antibody was first used to examine the phosphorylation states of Ser-150 in the liver after 12-h fasting. Fasting for 12 h induced a band shift of GRP58LIS (Fig. 3Aa) and increased the immunoreactivity of a band migrating at 60 kDa to anti-phosphoGRP58 antibody in 1DE (Fig. 3Ab). Furthermore, when anti-phosphoGRP58 antibody was preabsorbed with the antigen (EFKKFIpSDKDASC), immunoreactivity to the anti-phosphoGRP58 antibody disappeared in 1DE (Fig. 3Ac). Immunoreactivity to this anti-phosphoGRP58 antibody was observed only in the spots corresponding to 1-3 and 1-4 in 2DE (Fig. 3B). In controls, anti-phosphoGRP58 was preabsorbed to the antigen (EFKKFIpSDKDASC), which eliminated all immunoreactivity to anti-phosphoGRP58 in 2DE (data not shown). Three hours after interacranial injection of leptin immunoreactivity to anti-phosphoGRP58 increased in both 1DE or 2DE (spots 1-3 and 1-4) (data not shown). These observations indicate that 12-h fasting

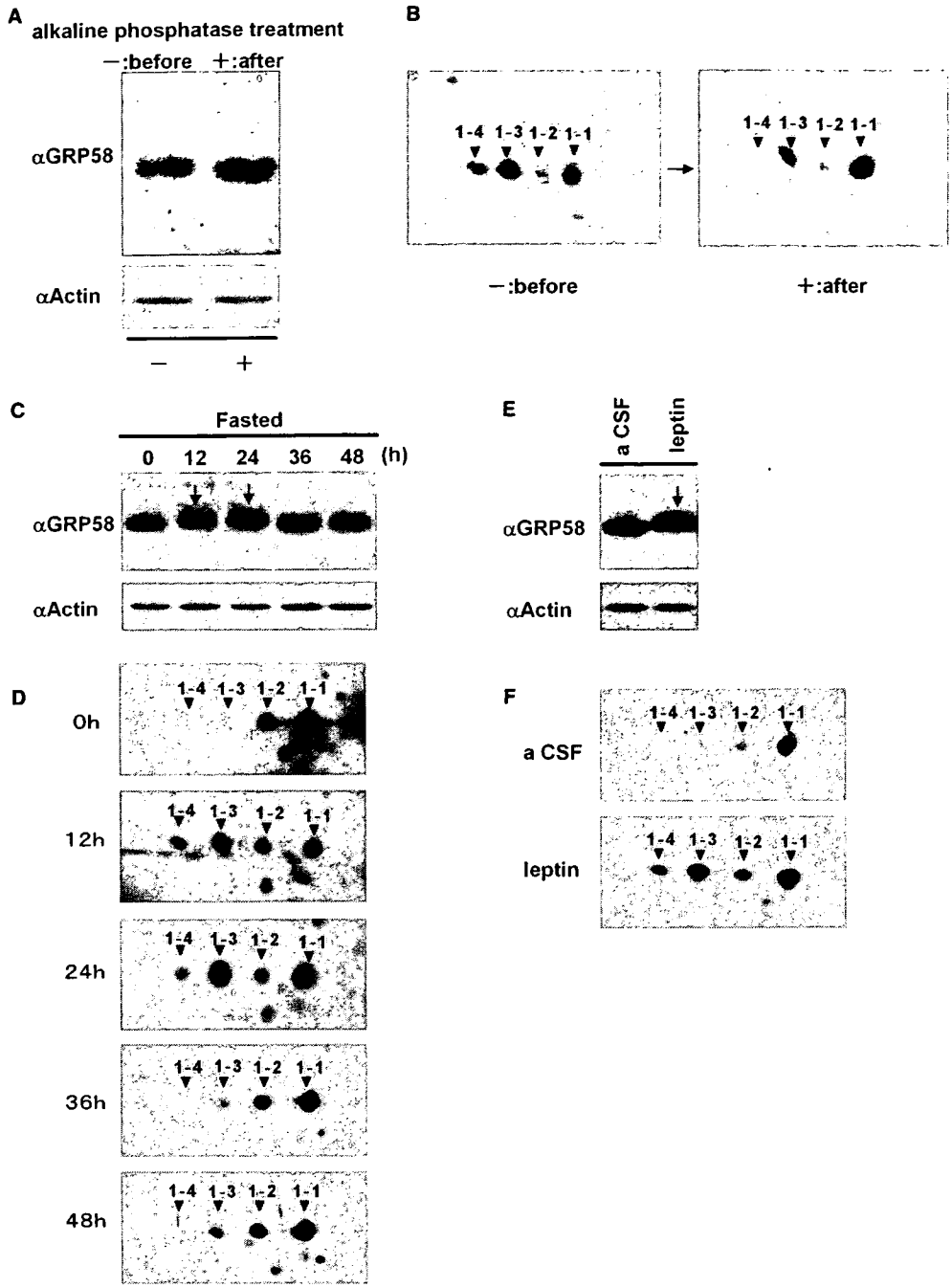

Fig. 2. Mobility changes in 1DE (A) and 2DE (B) after phosphatase treatment (A, B), fasting (C, D), and leptin injection (E, F). (A, B) Liver samples were obtained from rats at ZT11 and immunoblot analyses were carried out using anti-GRP58 antibodies before and after treatment with alkaline phosphatase in 1DE (A) and 2DE (B). (C, D) Effect of fasting on GRPLIS. Livers were obtained from rats at 0, 12, 24, 36 and 48 h after the start of food deprivation, homogenized and loaded onto 1DE and 2DE gels. After electrophoresis, immunoblot analyses were performed using an anti-GRP58 antibodies in 1DE (C) and 2DE (D). (E, F) Effect of leptin on GRP58LIS. Liver samples were obtained 3 h after the administration of leptin or aCSF and immunoblot analyses performed using an anti-GRP58 antibodies in 1DE (E) and 2DE (F).

and intracranial injection of leptin elevate phosphorylation of Ser-150 of GRP58.

To examine the possible role of GRP58 phosphorylation at aa 150 in intracellular signal transduction, an immunoprecipitation study was carried out using mouse anti-STAT3 monoclonal antibody. In an control experiment, it was observed that GRP58 was not precipitated with an anti-BIT (brain immunoglobulin-like molecule with tyrosine-based activation motifs) monoclonal antibody; 1D4, which is kindly given by Dr. Shin-ichiro Sano (Mitsubishi Kasei Industitute of Life Sciences, Japan) [12]. Therefore, above observation seems to be specific.

In this experiment, liver samples were obtained 3 h after the intracranial injection of leptin or aCSF and immunoreactivities to anti-GRP58 and anti-phosphoGRP58 antibodies were examined. As seen in Fig. 3C, immunoprecipitation using anti-STAT3 antibody precipitated GRP58LIS in the livers of rats injected with either leptin or aCSF. However, the immu-

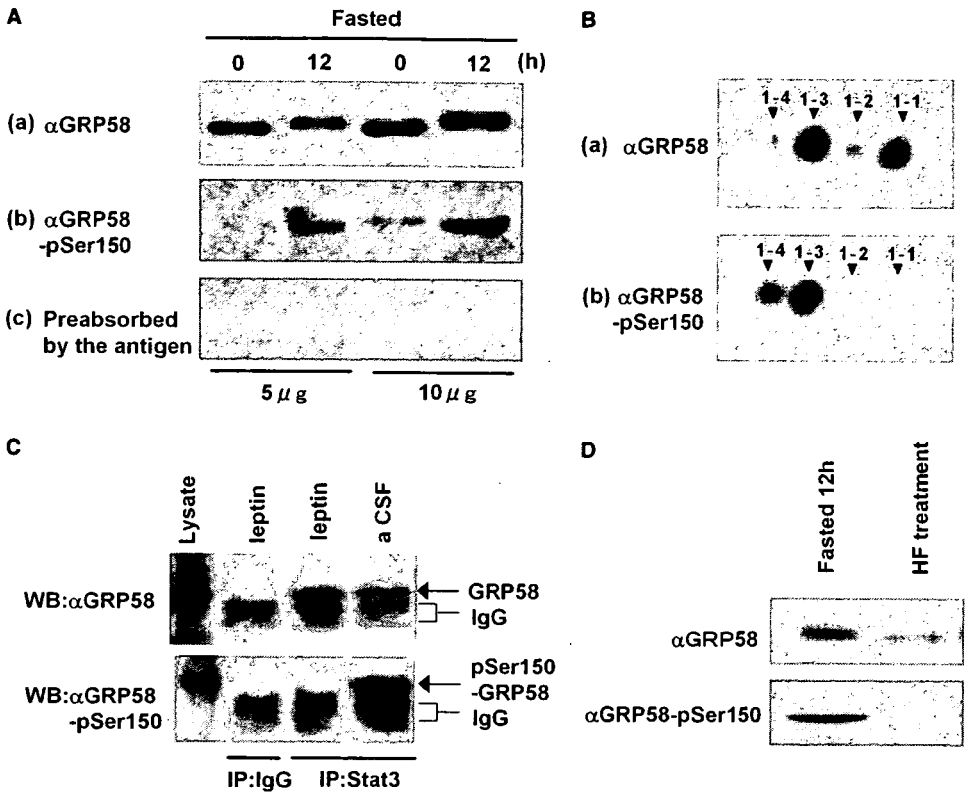

Fig. 3. Changes in immunoreactivity to anti-phosphoGRP58 antibody due to fasting and intracranial injection of leptin. (A, B) Immunoblot analyses of liver samples obtained at 0 and 12 h fasting using an anti-GRP58 and anti-phosphoGRP58 antibodies in 1DE (A) and 2DE (B). Specificity of the anti-phosphoGRP58 antibody was confirmed by preabsorbing it with the antigen. (C) Immunoprecipitation studies using anti-STAT3 antibody and IgG. Liver samples were obtained from rats 3 h after injections of leptin and aCSF and analyzed via immunoblotting. (D) Effect of dephosphorylation of GRP58 using hydrogen fluoride–pyridine on anti-GRP58 and anti-phosphoGRP58 immunoreactivity in livers obtained after 12-h fasting.

noreactivity to anti-phopshoGRP58 was immunoprecipitated by the anti-STAT3 antibody in the liver of aCSF-injected rats but not in that of leptin-injected rats, which indicates that the GRP58 phosphorylated at serine 150 is not able to bind STAT3.

To confirm the phosphorylation of GRP58 after fasting for 12 h, the effect of a dephosphorylation treatment using 70% hydrogen fluoride–pyridine on the immunoreactivity to anti-phosphoGRP58 antibodies in rats was examined. As seen in Fig. 3D, the immunoreactivity to the anti-phosphoGRP58 observed in rats fated for 12 h, disappeared following treatment with hydrogen fluoride–pyridine. This observation also confirms that GRP58 is phosphorylated at aa 150 after fasting.

4. Discussion

In this study, proteins showing daily changes in their rat liver expression patterns were identified via proteome analysis using 2DE and mass spectrometry. As a result, time-dependent changes in protein spots were detected with GRP58 being identified as one of the protein spots showing daily changes (Fig. 1; Table 1). GRP58 is a stress protein that is localized in the lumen of the endoplasmic reticulum because the C-terminus has an ER-retention signal. It is thought to be important for disulfide bond formation of proteins in the endoplasmic reticulum [13–15]. Recent data confirms the association between GRP58 and STAT3 in cytosolic statsome I complexes and indicates that both GRP58 and STAT family members co-associate in the plasma membrane compartment [4]. Thus, it is speculated that GRP58 might regulate signal transduction by sequestering active and inactive STAT3.

Therefore, it was of interest to characterize the daily changes in GRP58 expression in the rat liver. Although no daily change in the amount of GRP58LIS was observed, a shift in its mobility was observed at ZT11 in 1DE (Fig. 1B). Four GRP58LIS spots with similar molecular sizes but with different isoelectric points were observed in a time-dependent manner by immunoblotting in 2DE (Fig. 1C). Since horizontal scattering of spots in 2DE derived from the same protein with similar molecular weight is often the result of protein phosphorylation, it was hypothesized that GRP58 in the rat liver might be time-dependently phosphorylated in a time-dependent manner. This hypothesis was tested by examining the effect of an alkaline phosphatase on the migration of GRP58LIS obtained from liver samples at ZT11 in 1DE and 2DE. The phosphatase treatment slightly increased the mobility of GRP58LIS in 1DE (Fig. 2A) and reduced the immunoreactivities of the two GRP58LIS spots on the more acidic side (1-3 and 1-4) while enhancing the immunoreactivity of the spot on the most alkaline side (1-1) in 2DE gel (Fig. 2B). Altogether, these findings suggest that GRP58 is phosphorylated at ZT11.

Since ZT11 is almost at the end of the light period, it was possible that the mobility changes of GRP58 in 1DE and 2DE might be caused by food deprivation. This idea is supported by a recent report showing changes in the mobility of

ERp57 (GRP58) during recovery from ATP depletion using a cell culture based reversible ATP depletion model [16]. Therefore, the effect of food deprivation on the mobility of GRP58 was examined. As seen in Fig. 2C and D, food deprivation for 12 and 24 h caused a shift in the mobility of GRP58LIS in 1DE and increased the immunoreactivity of GRP58LIS on the acidic side (1-3 and 1-4 in Fig. 2D) in 2DE. These results indicate that GRP58 is phosphorylated after 12- and 24-h fasting. Glycogenolysis and gluconeogenesis in the liver are induced at ZT11 and after certain periods of fasting. Thus, the phosphorylation of GRP58 might be related to the mechanism of these processes.

As mentioned above, GRP58 is known to interact with STAT3 [4] and is thought to be involved in the intracellular signal transduction of leptin. As leptin might induce phosphorylation of GRP58, the effect of intracranial injection of leptin on the mobility of GRP58LIS in 1DE and 2DE was examined. Leptin induced a mobility shift of GRP58LIS in 1DE (Fig. 2E) and increased the immunoreactivities of GRP58LIS on the more acidic side in 2DE (1-3 and 1-4 in Fig. 2F), suggesting that GRP58 phosphorylation is induced by leptin.

Phosphorylation of GRP58 was found to occur at Ser150 after 12-h fasting and leptin injection. Moreover, it was found that dephosphorylation of GRP58 using hydrogen fluoride–pyridine eliminated immunoreactivity to anti-phosphoGRP58 antibody in liver samples obtained from rats fasted for 12 h (Fig. 3D). This observation confirmed that fasting induces phosphorylation of GRP58.

Immunoprecipitation using anti-STAT3 antibody (Fig. 3C) indicated that phosphorylation of GRP58 at Ser150 renders in unable to bind to STAT3. Since it has been suggested that GRP58 and STAT3 co-associate in the plasma membrane compartment [4], it is possible that unphosphorylated, but not phosphorylated GRP58 binds to STAT3. Thus, phosphorylation of GRP58 at Ser150 may constitute the signal that frees STAT3 from the plasma membrane compartment, resulting in the activation of the downstream signal transduction pathway. In this respect, it was found that GRP58 is present in STAT3-DNA complexes within the nucleus and is a necessary component them [17], suggesting that GRP58 is related to the nuclear entry and transcriptional regulation of STAT3.

In the current report, it is known that GRP58 of rat spleen is phosphorylated in three tyrosines (Y 444, Y 453 and Y466) by the Src-like tyrosine kinase Lyn [18]. Therefore, it is possible that spots of 1-1 and 1-2 may represent different phosphorylation states of these tyrosine residues.

These possibilities will be examined in future studies together with analyses of the constituents of spots 1-1 and 1-2, and of kinase responsible for the phosphorylation of aa 150 of GRP58.

References

[1] Lee, A.S. (1987) Coordinated regulation of a set of genes by glucose and calcium ionophores in mammalian cells. Trends Biochem. Sci. 12, 20–23.

[2] Mazzarella, R.A., Marcus, N., Haugejorden, S.M., Balcarek, J.M., Baldassare, J., Roy, B., Li, L.J., Lee, A.S. and Green, M. (1994) Erp61 is GRP58, a stress-inducible luminal endoplasmic reticulum protein, but is devoid of phosphatidylinositide-specific phospholipase C activity. Arch. Biochem. Biophys. 308, 454–460.

[3] Hirano, N., Shibasaki, F., Sakai, R., Tanaka, T., Nishida, J., Yazaki, Y., Takenawa, T. and Hirai, H. (1995) Molecular cloning of the human glucose-regulated protein ERp57/GRP58, a thiol-dependent reductase. Identification of its secretory form and inducible expression by oncogenic transformation. Eur. J. Biochem. 234, 336–342.

[4] Guo, G.G., Patel, K., Kumar, V., Shah, M., Fried, V.A., Etlinger, J.D. and Sehgal, P.B. (2002) Association of the chaperone glucose-regulated protein 58 (GRP58/ER-60/ERp57) with Stat3 in cytosol and plasma membrane complexes. J. Interferon Cytokine Res. 22, 555–563.

[5] Ndubuisi, M.I., Guo, G.G., Fried, V.A., Etlinger, J.D. and Sehgal, P.B. (1999) Cellular physiology of STAT3: Where's the cytoplasmic monomer?. J. Biol. Chem. 274, 25499–25509.

[6] Sehgal, P.B., Guo, G.G., Shah, M., Kumar, V. and Patel, K. (2002) Cytokine signaling: STATS in plasma membrane rafts. J. Biol. Chem. 277, 12067–12074.

[7] Schibler, U. (2003) Liver regeneration clocks on. Science 302, 234–235.

[8] Chun, S., Niijima, A., Nagai, N. and Nagai, K. (1998) Effect of bilateral lesions of the suprachiasmatic nucleus on hyperglycemia caused by 2-deoxy-D-glucose and vasoactive intestinal peptide in rats. Brain Res. 809, 165–174.

[9] Kuyama, H., Toda, C., Watanabe, M., Tanaka, K. and Nishimura, O. (2003) An efficient chemical method for dephosphorylation of phosphopeptides. Rapid Commun. Mass Spectrom. 17, 1493–1496.

[10] Schwartz, M.W., Woods, S.C., Porte Jr., D., Seeley, R.J. and Baskin, D.G. (2000) Central nervous system control of food intake. Nature 404, 661–671.

[11] Blom, N., Gammeltoft, S. and Brunak, S. (1999) Sequence and structure-based prediction of eukaryotic protein phosphorylation sites. J. Mol. Biol. 294 (5), 1351–1362.

[12] Sano, S., Matsuda, Y. and Nakagawa, H. (1989) A novel brain-specific antigen: a glycoprotein electrophoretically similar to but immunochemically different from type B nucleoside diphosphatase. J. Biochem. 105, 457–460.

[13] Murthy, M.S. and Pande, S.V. (1994) A stress-regulated protein. GRP58, a member of thioredoxin superfamily, is a carnitine palmitoyltransferase isoenzyme. Biochem. J. 304, 31–34.

[14] Koivunen, P., Horelli-Kuitunen, N., Helaakoski, T., Karvonen, P., Jaakkola, M., Palotie, A. and Kivirikko, K.I. (1997) Structures of the human gene for the protein disulfide isomerase-related polypeptide ERp60 and processed gene and assignment of these genes to 15q15 and 1q21. Genomics 42, 397–404.

[15] Lindquist, J.A., Jensen, O.N., Mann, M. and Hammerling, G.J. (1998) ER-60, a chaperone with thiol-dependent reductase activity involved in MHC class I assembly. EMBO J. 17, 2186–2195.

[16] Kumar, Y. and Tatu, U. (2003) Stress protein flux during recovery from simulated ischemia: induced heat shock protein 70 confers cytoprotection by suppressing JNK activation and inhibiting apoptotic cell death. Proteomics 3, 513–526.

[17] Margherita, E., Sabina, C., Fabio, A., Caterina, G., Anna, F. and Carlo, T. (2004) ERp57 is present in STAT3-DNA complexes. Biochem. Biophys. Res. Commun. 323, 1306–1312.

[18] Donella-Deana, A., James, P., Staudenmann, W., Cesaro, L., Marin, O., Brunati, A.M., Ruzzene, M. and Pinna, L.A. (1996) Isolation from spleen of a 57-kDa protein substrate of the tyrosine kinase Lyn. Identification as a protein related to protein disulfide-isomerase and localization of the phosphorylation sites. Eur. J. Biochem. 235, 18–25.

Available online at www.sciencedirect.com
ScienceDirect
ELSEVIER
Biochemical and Biophysical Research Communications 352 (2007) 579–586
BBRC
www.elsevier.com/locate/ybbrc

Evaluation of laser microdissection as a tool in cancer glycomic studies

Hiroaki Korekane [a,b], Kyoko Shida [a,b], Kohei Murata [c], Masayuki Ohue [c], Yo Sasaki [c], Shingi Imaoka [c], Yasuhide Miyamoto [a,*]

[a] *Department of Immunology, Osaka Medical Center for Cancer and Cardiovascular Diseases, 1-3-2 Nakamichi, Higashinari-ku, Osaka 537-8511, Japan*
[b] *Japan Health Sciences Foundation, 13-4 Nihonbashi Kodenma-cho, Chuo-ku, Tokyo 103-0001, Japan*
[c] *Department of Surgery, Osaka Medical Center for Cancer and Cardiovascular Diseases, 1-3-3 Nakamichi, Higashinari-ku, Osaka 537-8511, Japan*

Received 18 October 2006
Available online 14 November 2006

Abstract

Laser microdissection (LMD) is a recent development that enables the isolation of specific cell populations from tissue sections. This study focuses on the potential of LMD as a tool in cancer glycomics using colon cancer as a model. LMD was performed on hematoxylin and eosin stained frozen tissue sections. Tumor cells and normal epithelial cells were selectively microdissected. *N*-Glycans from the LMD- and the bulk tissue-derived samples were liberated by hydrazinolysis and then labeled with 2-aminopyridine. After sialidase digestion, the resulting asialo-*N*-glycans were analyzed by normal and reversed phase HPLC combined with mass spectrometry. Comparison of the various *N*-glycan profiles with the aid of LMD identified seven characteristic *N*-glycans with significantly different expression profiles between normal and cancerous cells that could not be detected by conventional analysis. Thus, LMD is a potent and useful tool for analyzing variations in the expression of *N*-glycans by overcoming the problem of tissue sample heterogeneity.

Keywords: Colon cancer; Glycomics; Microdissection; *N*-Glycans; Pyridylamination

It is well known that glycans on the cell surface or in the extracellular space play important roles in cellular differentiation, adhesion, and proliferation [1,2]. The biosynthesis of glycans is tissue-specific and is regulated not only by physiological conditions, but also by pathological conditions such as tumorgenesis [3–5]. Aberrant glycosylation of membrane components occurs in essentially all types of human cancers, and many glycosyl epitopes constitute tumor-associated carbohydrate antigens (TACAs) [6–8]. Many lines of evidence suggest that the TACAs function mainly as adhesion molecules and contribute to cancer metastasis [7,9–11]. Alteration of the expression profile of TACAs in certain types of cancer has prompted researchers to evaluate their potential use as diagnostic and/or prognostic tools.

The application of glycomics to cancer research can highlight changes in the expression profile of the glycans occurring during tumor development and progression, leading to the identification of new molecular markers or potential therapeutic targets. However, because cancer tissue is composed of multiple subpopulations of cells, including normal epithelial cells, stromal cells, inflammatory cells, and angiogenic elements, accurate molecular analysis requires isolation of the tumor cells. Laser microdissection (LMD) is a recently developed technique that permits the reliable procurement of specific cell populations from tissue sections under direct microscopic observation. The laser-assisted microdissection technique has already been extensively used to isolate specific types of cells for the molecular analysis of DNA, RNA, and protein. However, in the field of glycan research, only one application of this technique for the analysis of glycosaminoglycans in postmortem human LASIK corneas has been reported [12]. Because LMD is a highly time consuming technique, feasibility

* Corresponding author. Fax: +81 6 6972 7749.
E-mail address: miyamoto-ya@mc.pref.osaka.jp (Y. Miyamoto).

0006-291X/$ - see front matter © 2006 Elsevier Inc. All rights reserved.
doi:10.1016/j.bbrc.2006.10.191

and usefulness of this procedure must be thoroughly evaluated prior to its application in the analysis of glycans in cancer specimens.

In this study, we have investigated the potential of LMD as a tool in cancer glycomic studies using colon cancer as a model. Asialo-PA-*N*-glycans were prepared from bulk colon cancer tissue, bulk normal colon tissue, and from both normal colonic epithelial cells and cancerous colonic cells isolated from the bulk tissue using LMD. The *N*-glycans were then analyzed by normal and reversed phase HPLC in combination with mass spectrometry. LMD enabled us to identify seven characteristic *N*-glycans which displayed remarkable differences in the expression profile between normal and cancerous colon cells that could not be detected by conventional techniques. Our results demonstrate the usefulness of LMD for the accurate analysis of *N*-glycans in cancer glycomic studies.

Materials and methods

Standard PA-oligosaccharides. The structures and abbreviations of the authentic PA-oligosaccharides used in this study are listed in Table 1. Authentic PA-sugars were obtained from the following suppliers: 224F from Takara (Shiga, Japan); 22bis, ag22bisF, $G_1$22bisF, and 22bisF from Seikagaku Co. (Tokyo, Japan). Ag22bis was prepared by digestion of 22bis with Jack bean β-galactosidase (Seikagaku Co.). The structure of ag22bis was verified by normal and reversed phase HPLC analyses, combined with successive exoglycosidase digestions and by mass spectrometric analysis.

Tissue. Paired samples of normal and cancerous colon were obtained from the same patient by a standard colectomy procedure. Areas of tissues examined were selected by an experienced gastrointestinal pathologist. The tissue was cut into blocks, embedded in OCT compound (Sakura Finetechnical, Tokyo, Japan), snap frozen in liquid nitrogen, and stored at −80 °C until use. This study was approved by Local Ethics Committee of Osaka Medical Center for Cancer and Cardiovascular Diseases. Informed consent was obtained from the patient.

Laser microdissection. Frozen tissue sections (8 μm thick) of either cancerous colon or normal colonic mucosa were cut on a cryostat, CM 1900 microtome (Leica, Milton Keynes, UK). Tissue sections were thaw mounted on to a film-coated glass slide (90FOIL-SL25, Leica), briefly air dried, and then fixed at room temperature in 95% ethanol for 1 min. Staining was performed by the following procedure. Sections were immersed in Mayer's hematoxylin solution (Muto Pure Chemicals, Tokyo, Japan) for 30 s at room temperature, washed with phosphate-buffered saline (PBS) until a vivid blue color appeared, and then immersed in pure eosin solution (Muto Pure Chemicals) for 2 s. The sections were then dehydrated in 100% ethanol for 30 s and air dried. Laser microdissection (LMD) was performed using a Leica AS LMD system.

Preparation of protein extracts. After microdissection, the microdissected cells were carefully transferred from a PCR tube to a glass centrifuge tube using water and a micropipette. The collected cells were lyophilized and then solubilized in a 1:1 mixture of hexafluoroisopropanol (HFIP) [13,14] and 0.2% acetic acid. Control samples, which had not been subjected to LMD, were prepared from the frozen tissue sections cut directly into the solubilization mixture. The protein concentration was determined with a BCA protein assay kit (Pierce, Rockford, IL) using bovine serum albumin as a standard. A protein sample of 300 μg was collected, concentrated, and used for the preparation of PA-*N*-glycans.

Preparation of PA-N-glycans. *N*-Glycans were liberated from the glycoproteins by hydrazinolysis at 100 °C for 10 h and then re-*N*-acetylated with acetic anhydride in a saturated sodium bicarbonate solution as previously described [15]. The reducing ends of the liberated *N*-glycans were labeled with a fluorophore, 2-aminopyridine, by reductive amination [16]. The excess reagents were removed by phenol–chloroform extraction and cation-exchange chromatography [17]. The resulting PA-*N*-glycans were further purified by normal phase HPLC according to the method of Nakakita et al. [18] with minor modifications. Briefly, the lyophilized PA-*N*-glycans were dissolved in water and then injected into a TSKgel Amide-80 column (4.6 × 75 mm, Tosoh, Tokyo, Japan). The solvents used were

Table 1
Structures and elution positions in HPLC of standard PA-oligosaccharides

Abbreviation	Structure	Elution position in HPLC	
		RP (GU)	NP (GU)
ag22bis	GlcNAcβ1-2Manα1(6) GlcNAcβ1-4Manβ1-4GlcNAcβ1-4GlcNAc-PA GlcNAcβ1-2Manα1(3)	11.45	5.37
22bis	Galβ1-4GlcNAcβ1-2Manα1(6) GlcNAcβ1-4Manβ1-4GlcNAcβ1-4GlcNAc-PA Galβ1-4GlcNAcβ1-2Manα1(3)	12.72	6.78
ag22bisF	GlcNAcβ1-2Manα1(6) Fucα1(6) GlcNAcβ1-4Manβ1-4GlcNAcβ1-4GlcNAc-PA GlcNAcβ1-2Manα1(3)	14.90	5.66
$G_1$22bisF	Galβ1-4GlcNAcβ1-2Manα1(6) Fucα1(6) GlcNAcβ1-4Manβ1-4GlcNAcβ1-4GlcNAc-PA GlcNAcβ1-2Manα1(3)	15.86	6.29
22bisF	Galβ1-4GlcNAcβ1-2Manα1(6) Fucα1(6) GlcNAcβ1-4Manβ1-4GlcNAcβ1-4GlcNAc-PA Galβ1-4GlcNAcβ1-2Manα1(3)	16.80	7.02
224F	Galβ1-4GlcNAcβ1-2Manα1(6) Fucα1(6) Galβ1-4GlcNAcβ1(4)(3)Manβ1-4GlcNAcβ1-4GlcNAc-PA Galβ1-4GlcNAcβ1(2)Manα1	13.91	7.96

(A) 90% acetonitrile–3% acetic acid titrated to pH 7.3 with triethylamine and (B) 20% acetnitrile–3% acetic acid titrated to pH 7.3 with triethylamine. Elution was performed at a flow rate of 1.0 ml/min at 40 °C. The column was equilibrated with solvent A, and after injection of a sample, the following gradient was employed: 0–28% B over 7 min; 28–100% B over 5 min; 100% B for 4 min. PA-*N*-glycans were detected with a fluorescence spectrophotometer using excitation and emission wavelengths of 310 and 380 nm, respectively. The fraction between 7 and 16 min after the injection was collected, concentrated, and used for the structural studies.

Preparation and size-fractionation of asialo-PA-N-glycans. PA-*N*-glycans were dissolved in 50 μl of 100 mM ammonium acetate buffer (pH 5.0) and then digested with 2 U/ml of *Arthrobacter ureafaciens* neuraminidase (Nacalai Tesque, Kyoto, Japan) at 37 °C for 24 h. The reaction was terminated by boiling for 3 min, followed by centrifugation at 13,000*g* for 10 min. The resulting supernatant was injected into a normal phase HPLC apparatus equipped with a TSKgel Amide-80 column (4.6 × 75 mm), and the asialo-PA-*N*-glycans were size-fractionated into nine fractions from glucose unit (GU) 3 to GU12 at intervals of one glucose unit, according to the method of Fujimoto et al. [19] with some modifications. The solvents used were (A) 90% acetonitrile–0.6% acetic acid titrated to pH 7.3 with triethylamine and (B) 20% acetnitrile–0.6% acetic acid titrated to pH 7.3 with triethylamine. The elution was performed at 40 °C using a flow rate of 1 ml/min. The column was equilibrated with 5% solvent B, and after injection of a sample, solvent B was increased linearly to 75% in 25 min. The PA-*N*-glycans were detected using excitation and emission wavelengths of 310 and 380 nm, respectively.

HPLC for structural analysis. Reversed phase HPLC was performed at 30 °C on a Cosmosil $3C_{18}$-P column (2 × 100 mm, Nacalai Tesque) at a flow rate of 0.2 ml/min. The solvents used were (A) 20 mM ammonium acetate buffer pH 4.0 and (B) the same buffer containing 0.5% 1-butanol. The column was equilibrated with 5% solvent B, and after injection of a sample, solvent B was linearly increased to 100% over 50 min and then held at 100% for 3 min. Fluorescence was monitored using excitation and emission wavelengths of 320 and 400 nm, respectively.

Normal phase HPLC was performed at 40 °C on a TSKgel Amide-80 (2 × 150 mm, Tosoh) at a flow rate of 0.2 ml/min. The solvents used were (A) 90% acetonitrile–0.6% acetic acid titrated to pH 7.3 with triethylamine and (B) 20% acetnitrile–0.6% acetic acid titrated to pH 7.3 with triethylamine. The column was equilibrated with 5% solvent B, and after injection of a sample, solvent B was linearly increased to 75% over 40 min. Fluorescence was monitored using excitation and emission wavelengths of 310 and 380 nm, respectively.

The structures of the PA-glycans were assessed by two-dimensional sugar chain mapping [20–22]. The retention time of each of PA-glycans was given in glucose unit based on the elution time of the PA-isomaltooligosaccharides. The behavior of authentic PA-oligosaccharides on HPLC is shown in **Table 1**.

Glycosidase digestion for structural analysis. PA-glycans were digested in a volume of 20 μl for 16 h at 37 °C using the following enzymes: *Streptococcus pneumoniae* β-galactosidase (Prozyme, San Leandro, CA), specificity for β(1,4)Gal, 0.1 U/ml in 50 mM sodium acetate buffer, pH 5.6; *Streptomyces* sp.142 α-fucosidase (Takara), specificity for α(1,3/4)Fuc, 0.2 mU/ml in 50 mM potassium phosphate buffer, pH 6.0.

NanoESI ion-trap mass spectrometry. Mass spectra of the PA-glycans were observed on a Finnigan LCQ Deca XP ion-trap mass spectrometer (Thermo Electron Co., Waltham, MA) equipped with a nanoESI device (AMR, Inc., Tokyo, Japan) connected to a Paradigm MS4 μHPLC system (Michrom BioResources, Inc., Auburn, CA). Reversed phase HPLC was performed at room temperature on a Magic C18 column (5 μm, 0.2 × 50 mm, Michrom BioResources) with a FortisTip capillary needle (AMR, Inc.) at a flow rate of 2 μl/min. The solvents used were (A) 5 mM acetic acid titrated to pH 6.0 with triethylamine and (B) 50% (v/v) methanol. The column was pre-equilibrated with solvent A, and 3 min after injection of a sample, solvent B was increased to 100% over 1 min and then held at 100% for 10 min. The nanoESI voltage was set at 1.8 kV and the capillary temperature was 200 °C.

Results

Tissue preparation for LMD

Hematoxylin and eosin (H&E) are the most commonly used histochemical stains. Good recovery (85%) of pyridylamino (PA) *N*-glycans was obtained after H&E

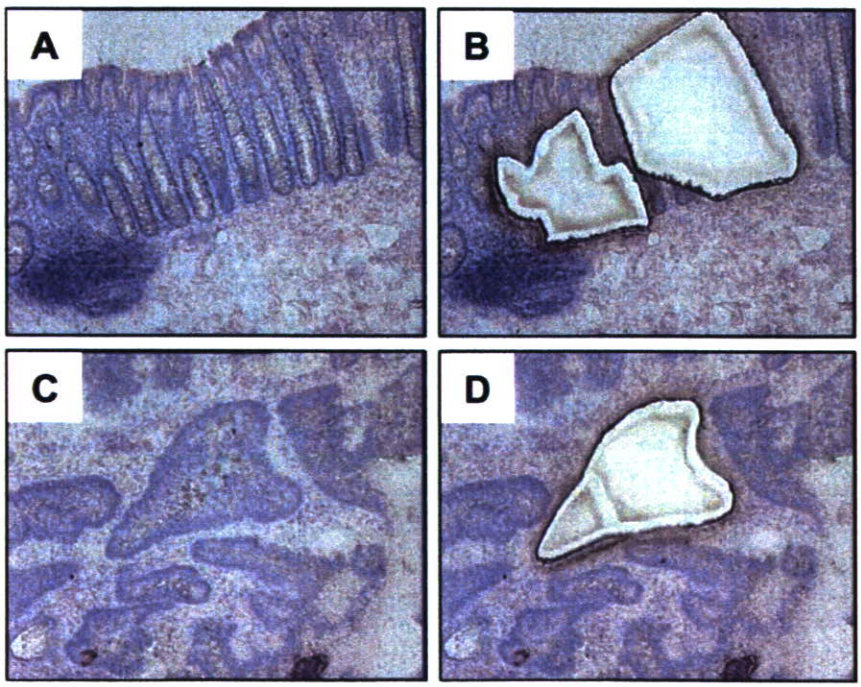

Fig. 1. Photomicrographs of laser microdissection of H&E stained tissue sections of normal colon (A,B) and cancerous colon (C,D). (A,C) Normal colon and cancerous colon, respectively, before microdissection. (B,D) Samples after successful microdissection. Representative data are shown.

staining and solubilization of the sections with 50% hexafluoroisopropanol (HFIP)/0.1% acetic acid mixture. Moreover, there was no gross effect on the resulting asialo-PA-*N*-glycans profile of colon cancer tissues (Supplementary Fig. 1). Thus, H&E staining and HFIP/acetic acid mixture were used for tissue preparation prior to LMD and for solubilization of samples, respectively. Colon cancer cells and normal colonic epithelial cells were successfully microdissected with the laser from the tumor and normal tissue sections, respectively, as shown in Fig. 1.

Comparison of N-glycan profiles from the LMD- and the bulk tissue-derived samples

PA-*N*-glycans were prepared from the LMD- or the bulk tissue-derived samples. After sialidase digestion, the resulting asialo-PA-*N*-glycans were separated into nine fractions (F1–F9) by normal phase HPLC (Fig. 2), in which oligosaccharides were separated in accordance with their molecular size. Each of the collected fractions was further separated by reversed phase HPLC. Comparison of the *N*-glycan profiles obtained from the LMD-derived samples with those from the bulk tissue-derived samples showed clear differences in fractions F2–F6 (Fig. 3). Although the expression profile of many *N*-glycans is different between normal and cancerous cells, we picked up 12 characteristic peaks (G1–G12) whose marked expression changes could only be detected using the LMD procedures. The detection of these peaks directly demonstrates the potential of using LMD to overcome problems associated with tissue heterogeneity. All 12 peaks displayed a substantial decrease in intensity in the cancerous colon cells relative to normal colon cells. Each of these peaks was fractionated and further purified by normal phase HPLC for structural analysis as described in Materials and methods. Elution positions of G1–G12 on normal and reversed phase HPLC are summarized in Fig. 4A as a two-dimensional map. Peaks G3, G5, G10, and G12 had the same positions on the map as G2, G4, G6, and G9, respectively, indicating that each paired peak possessed the same structure. These results presumably arose from incomplete separation during the initial size-fractionation step (Fig. 2). From the positions on the map corresponding to authentic PA-*N*-glycans (Table 1), G1, G2 (G3), G4 (G5), G6 (G10), and G9 (G12) were estimated to be ag22bis, ag22bisF, $G_1$22bisF, 22bisF, and 224F, respectively. These structures were also confirmed by mass analysis (Table 2). The structures of the peaks G7, G8, and G11 were determined by two-dimensional mapping combined with exoglycosidase digestion and mass spectrometry as follows.

Peaks G7 and G8, both of which had the same composition of $Hex_5HexNAc_5dHex_2$-PA (Table 2), were sequentially digested with exoglycosidases in following order: 1st *S. pneumoniae* β(1,4)-galactosidase, *S.* sp142 α(1,3/4)-fucosidase, and 2nd *S. pneumoniae* β(1,4)-galactosidase (Fig. 4B and Supplementary Table 1). A single residue was removed at each step, indicating the presence of one Lewis^x structure with fucose linked α(1,3) to GlcNAc (the presence of fucose rendering the galactose residue resistant to cleavage). Elution positions on the map of the digests were shifted to that corresponding to the authentic PA-*N*-glycans, $G_1$22bisF and ag22bisF, after digestion with the α-fucosidase and

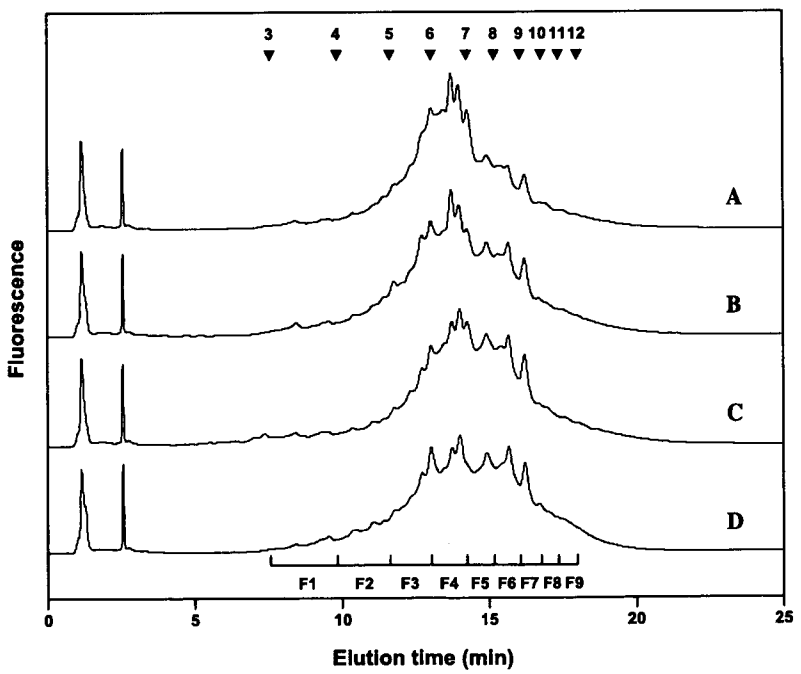

Fig. 2. Size-fractionation HPLC of asialo-PA-*N*-glycans from normal colon and colon cancer. (A,B) Normal and cancerous colon, respectively, which were not subjected to laser microdissection (LMD). (C,D) Normal and cancerous colon, respectively, which have been subjected to LMD to isolate normal epithelial cells and tumor cells. Numbered arrowheads indicate the elution position of PA-isomaltooligosaccharides with the corresponding degree of polymerization. Fractions F1–F9 were collected as indicated by the partitioned bars.

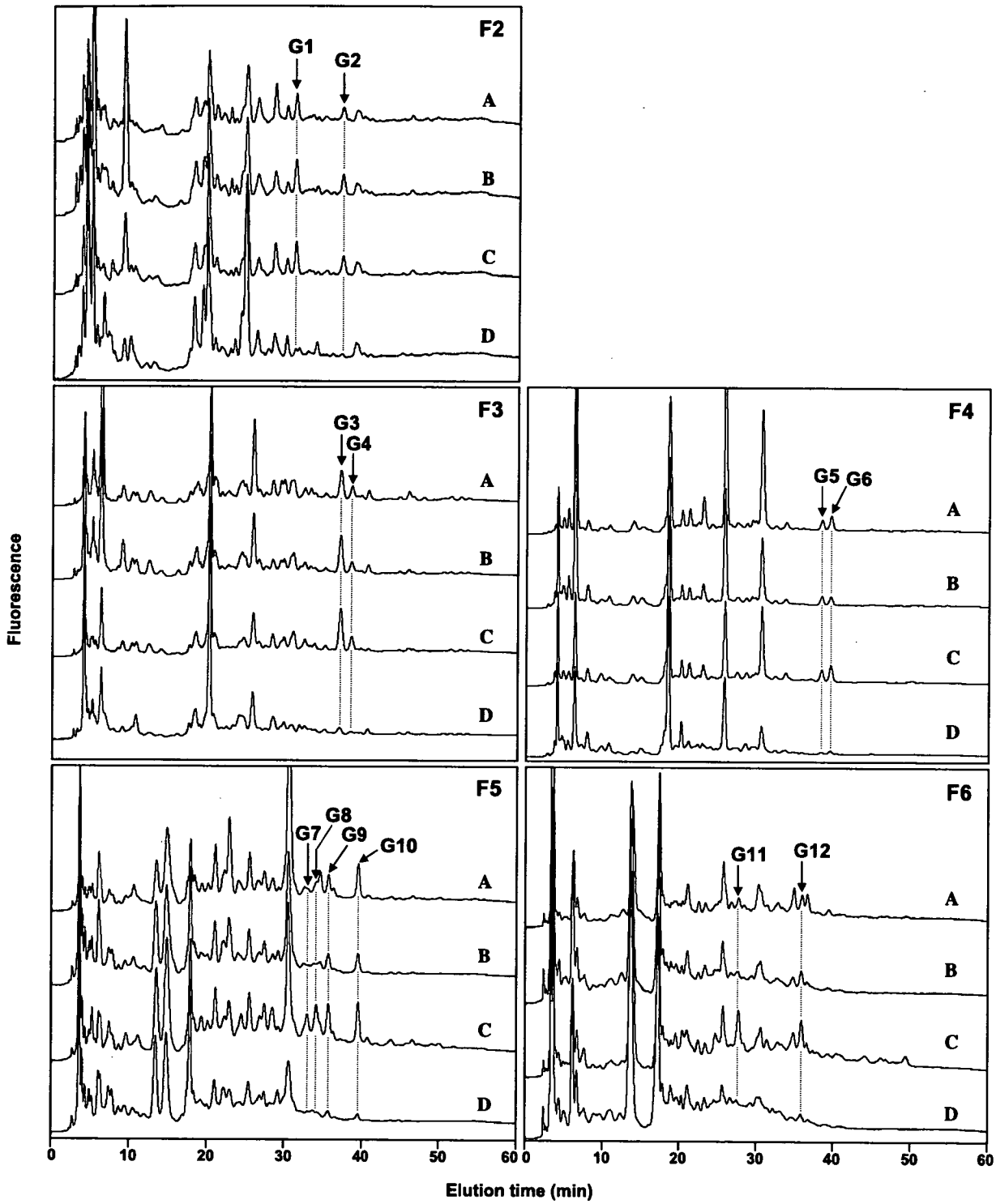

Fig. 3. Reversed phase HPLC profiles of the fractions F2–F6. (A,B) Normal and cancerous colon, respectively, which were not subjected to laser microdissection (LMD). (C,D) Normal and cancerous colon, respectively, which have been subjected to LMD. Twelve peaks (G1–G12) were collected.

the 2nd β-galactosidase, respectively. Thus the structures of these two peaks were estimated to be 22bisF with one Lewis^x structure.

Peak G11, which had the composition of $Hex_5HexNAc_5dHex_3$-PA (Table 2), was resistant to digestion with *S. pneumoniae* β(1,4)-galactosidase, but was sensitive to sequential digestion with *S.* sp142 α(1,3/4)-fucosidase followed by *S. pneumoniae* β(1,4)-galactosidase (Fig. 4B and Supplementary Table 1). Two residues were removed at each step indicating the presence of the two Lewis^x structures with fucose linked α(1,3) to GlcNAc. Elution positions on the map of the digests were shifted to that corresponding to the authentic PA-*N*-glycans, 22bisF and ag22bisF, after digestion with the α-fucosidase and the